SINGLET FISSION FOR PEROVSKITE SOLAR CELL

By

Toan Ngoc Le

Submitted to the graduate degree program in Mechanical Engineering and the Graduate Faculty of the University of Kansas in partial fulfillment of the requirements for the degree of Master of Science.

Chair: Dr. Lin Liu

Dr. Sara Wilson

Dr. Gibum Kwon

Date Defended: November 6, 2023

The thesis committee for Toan Ngoc Le certifies that this is the approved version of the following thesis:

SINGLET FISSION FOR PEROVSKITE SOLAR CELL

Chair: Dr. Lin Liu

Dr. Sara Wilson

Dr. Gibum Kwon

Date Approved: November 6, 2023

ABSTRACT

The perovskite solar cell has recently gained momentum within the renewable energy industry due to its unique advantages such as high efficiency and cost-effectiveness. However, its instability remains a challenge to its commercialization. In this study, a singlet fission material, namely tetracene, is coupled with the perovskite solar cell to simulate its effect on the solar cell. The amount of thermalization loss and the temperature of the perovskite layer are simulated and analyzed to indicate the mechanism's effectiveness. We found that coupling the tetracene layer resulted in a drastic reduction in thermalization loss and a slower slope in perovskite layer temperature. This indicates that tetracene would stabilize the perovskite solar cell and minimize its potential losses. The thickness of the solar cell layers is also analyzed as a factor of the overall effectiveness of singlet fission on solar cells.

ACKNOWLEDGEMENTS

I would like to express my gratitude for my academic advisor, Dr. Lin Liu for accepting me, as well as his guidance and support during my entire master program. His insights and expertise have been invaluable for me, as well as shaping my foundation as a researcher. I would also like to thank my committee members, Dr. Sara Wilson and Dr. Gibum Kwon for taking their time and giving feedback on my thesis. I also want to give my thanks to all of my KU professors and faculties, who have taught me valuable knowledge and helped me during my study.

Additionally, I am also deeply grateful to my parents, as well as my friends for their unwavering support and encouragement. Their encouragement has helped me a lot, especially mentally, for me to find strength to keep moving forward during the pandemic.

Dedication

To my parents, who raised me up and supported me,

To my friends, Dat, Hung, and Duy, who accepted me, and shares my interests,

To the future, where everything can be a bit kinder,

And to my future self, who may need encouragement to keep moving forward.

Table of contents

List of Figure

List of Tables

Nomenclature

Symbol	Definition
G^0	Solar spectral flux density
λ	Wavelength of light
G_{SC}	Solar constant
a	Modifier constant
E	Energy of photons

h	Planck's constant
c	Speed of light
ϕ	Number of photons
ϕ_1	Number of electrons of class P1
ϕ_2	Number of electrons of class P2
ϕ_3	Number of electrons of class P3
E_g	Band gap of the material
E_{P_2}	The energy level of photon class P2
E_{P_3}	The energy level of photon class P3
E_w	Thermalization energy loss
S_0	Grounded electron state of perovskite
S_1	Excited singlet electron state of perovskite
$E_{w_{control}}$	Wasted energy in the control case
S_0'	Grounded electron state of tetracene
R_1'	Triplet electron state of tetracene
E_w'	Wasted energy in the tetracene layer in the tetracene case
$E_{w_{SF}}$	Thermalization energy loss of tetracene layer in tetracene case
E_{w_P}	Thermalization energy loss of perovskite layer in tetracene case
ΔT_p	Change of temperature due to photon energy
m	Mass of the layer
τ	Specific heat of the material
Q_C	Heating due to heat transfer
ΔT_c	Temperature changes due to heat transfer
G	Equivalent thermal exchange coefficient
$G_{cd,i,j}$	Equivalent conductive thermal exchange coefficient between layer i and j
T_i	Temperature of layer i
ρ	Density of the material
S	Surface area of the material
d	Thickness of material
C	Thermal capacitance
C'	Capacitive contribution
γ	Thermal conductivity
G_{cv}	Equivalent convective thermal exchange coefficient
h_{conv}	Convection heat transfer coefficient
v_w	Wind speed
h_{free}	Free convection
h_{forced}	Forced convection
T_a	Ambient temperature
$G_{r,i,gro}$	Equivalent radiative thermal exchange coefficient with layer i and ground
ε_g	Emissivity of glass
$F_{i,gro}$	Configuration factor of layer i and the ground

$F_{i,sky}$	Configuration factor of layer i and the sky
σ	Stefan-Boltzmann's constant
T_{gro}	Temperature of the ground
T_{sky}	Temperature of the sky
β	Inclination
$\frac{dE_g}{dT}$	Change of bandgap with respect to temperature
$[\frac{dE_g}{dT}]_{TE}$	Change of bandgap due to thermal expansion
$[\frac{dE_g}{dT}]_{EP}$	Change of bandgap due to electron-phonon interactions
α_V	Volumetric expansion coefficient
B_0	Bulk modulus
$\frac{dE_g}{dP}$	Change of bandgap with respect to pressure
A_{eff}	Electron-phonon coupling constant
$\hbar\omega_{eff}$	Average phonon frequency
k_B	Boltzmann constant
$\%E_{below}$	Fraction of loss due to below-bandgap photons
$\%E_w$	Fraction of loss due to thermalization

1. Overview of Solar Cell

1.1 History of Solar Cell

The history of solar cells began in 1839 when Edmond Becquerel created the first photovoltaic cell, using silver chloride placed in acidic solution while it was connected to platinum electrodes. Years later, around 1877, W.G. Adams and R.E. Day demonstrated that electricity could be produced from light in selenium[1]. They called it "photoelectric", or as we call it "photovoltaic". The first solar module was then developed by Charles Edgar Fritts in 1833, and was then further improved by Gerald L. Pearson, Daryl M. Chaplin and Calvin S. Fuller at Bell Labs in 1954, using silicon instead of selenium.[2]

Shortly thereafter, the first commercial solar cell was available to purchase. However, the early models were costly, and the efficiency was poor, only around 6% when it was first made available[2]. Therefore, it was only seen used in programs where cost is not a critical issue, such as satellite projects. The field also did not receive much attention due to the cost, as well as the poor efficiency. It remained relatively small in energy production until the energy crisis in 1973, pushing the US government to be more invested in renewable energy. Alongside that, the field also received more attention as the population became more concerned with the negative environmental impact of coal and oil on the environment. Figure 1 captures the rising in popularity of solar energy within the renewable categories by the Energy Information Administration:

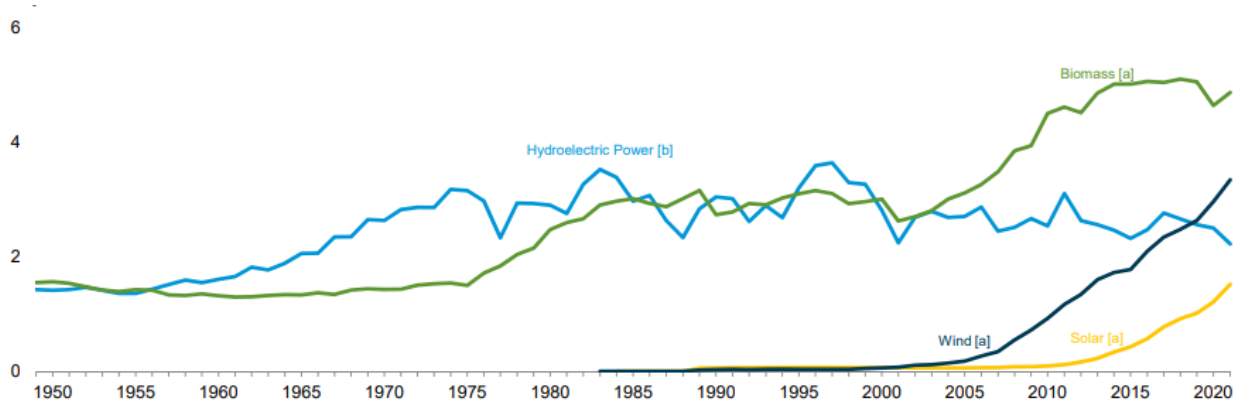

Figure 1: Renewable energy consumption

However, despite the rising in popularity, the market for solar energy is still relatively small, compared to other sources. Figure 2 describes the energy consumption in the United States from 1950 to 2020:

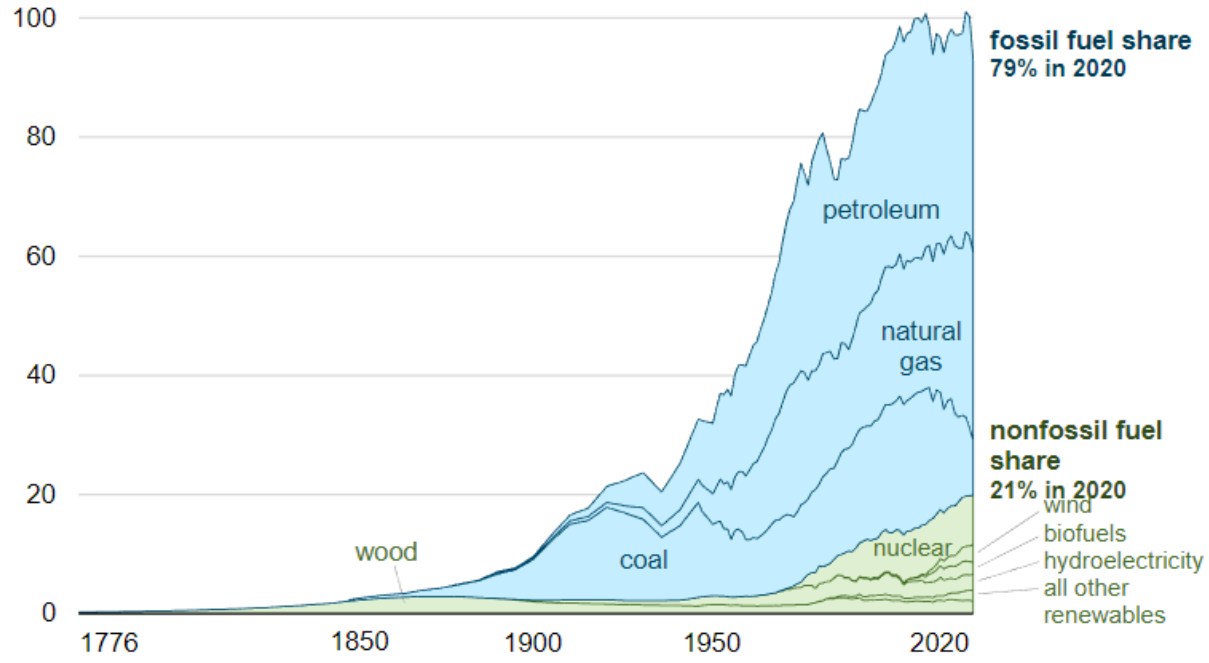

Figure 2: Energy consumption in the United States from 1950 to 2020 by types[3]

1.2. Basic function of a solar cell

Solar cells normally consist of 2 layers. One layer is doped with free electrons, called n-type doping, while the other is doped with holes, called p-type doping. For silicon, arsenic or phosphorus is added to make n-doped silicon layer, while boron or gallium is used in p-type doping. These two doped layers are then placed together to form a p-n junction. In a typical p-n junction, some of the free electrons from the N side near the interface will migrate to the P side to fill the available holes. This creates a depletion zone where there are no available free electrons and holes. Due to this migration, the N side becomes slightly positively charged, while the P side becomes slightly negatively charged. Because of this, an electric field will be formed between the layers. This electric field is necessary to produce the driving force necessary to form an electric flow necessary to create current. This is also the reason semiconductors are used instead of conductors, which conduct more easily.

When light strikes the solar panel, if the energy of the photon is sufficient to excite the electrons to cross the bandgap, an electron-hole pair is generated. The electric field will then drive the electron-hole pair out of the depletion zone, creating a potential difference between the two layers, ready to be connected to a load to produce electricity.

1.3. Bandgap

In materials, a bandgap is the distance between the valance band and the conduction band. In other words, the bandgap is the minimum energy required to excite an electron to become conductive. In most metals, the valance band and the conduction band overlap with each other. This is the reason most metals have high conductivity. On the other hand, in insulators, the bandgap value is large. This explains why insulators do not conduct electricity well. Meanwhile, semiconductors possess the bandgap of relatively small, in the range of 1-1.8eV. Figure 3 shows

the bandgap values of some of the popular semiconductors used in solar cell, as well as their respective efficiency:

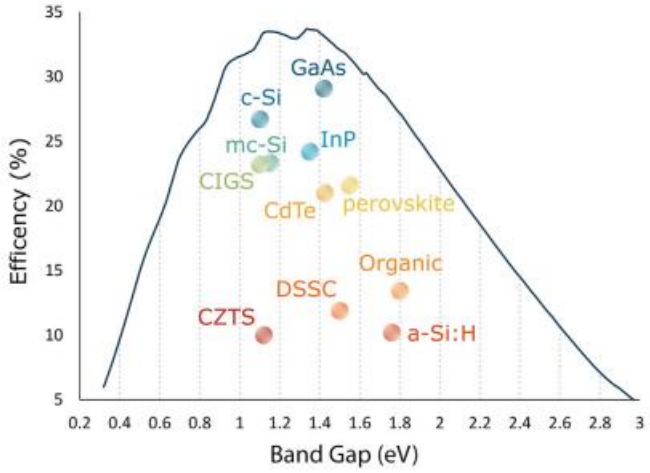

Figure 3: Efficiency and bandgap values of popular solar cells. Reprinted from Joule, Vol 4, Brandon R. Sutherland, Solar Materials Find Their Band Gap, Copyright (2023), with permission from Elsevier.

1.4. Shockley-Queisser limit

In solar cells, the photons absorbed are quantized. That means electron-hole pair in the solar cell will only absorb a set amount of energy for each photon to become excited. The amount of energy required is characterized by the bandgap of the semiconductor used in the solar cell. For example, Silicon has a bandgap value of 1.1eV. This means that every photon with an energy level less than 1.1eV (in the infrared region) is completely lost. In contrast, when the energy level of a photon surpasses the bandgap value, a process called thermalization will occur. In this process, the excess energy relaxes down to the band edge that is lost as heat (i.e., thermalization loss). In turn, the heat generated from this process causes the solar cell to heat up, which will cause it to degrade. These two kinds of loss in solar cell are characterized by the Shockley-Queisser limit[4]. It was calculated by William Shockley and Hans-Joachim Queisser in 1961. This limit represents the

maximum theoretical efficiency of a solar cell using a single p-n junction with respect to the bandgap of the semiconductor. In their analysis, the maximum solar conversion efficiency for solar cell is 33.4%, occurs at the bandgap of 1.34eV. Figure 3 shows the details of the aforementioned limit:

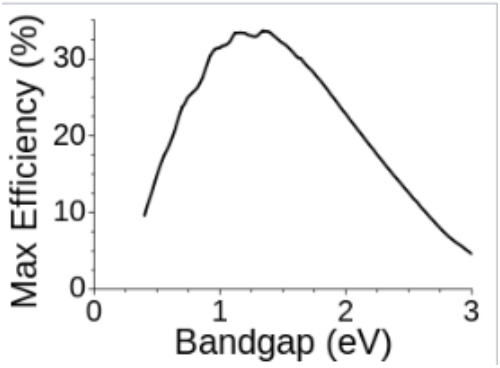

Figure 4: Shockley-Queisser limit

1.5. Stability

For a solar cell product to be able to be commercialized, it has to pass the requirements of the stability test, defined by the International Electrochemical Commission (IEC), or more specifically, the IEC 61646 standards. The guaranteed reliability required for many applications, from grid-connected PV systems to building-integrated photovoltaics (BIPV) is around 20 years of practical lifetime or longer[5]. In particular, these tests take the degradation behavior responding to irradiance and temperature exposure into account[5]. A more detailed discussion on the instability of our main subject, the perovskite solar cell, is included in later sections.

1.6. Commercialization

When the first solar panel was commercialized, the cost for solar energy was extremely high. Adjusting for inflation, it costed around $76 per watt for a solar module. Figure 5 depicts the price for conventional silicon solar cell over time:

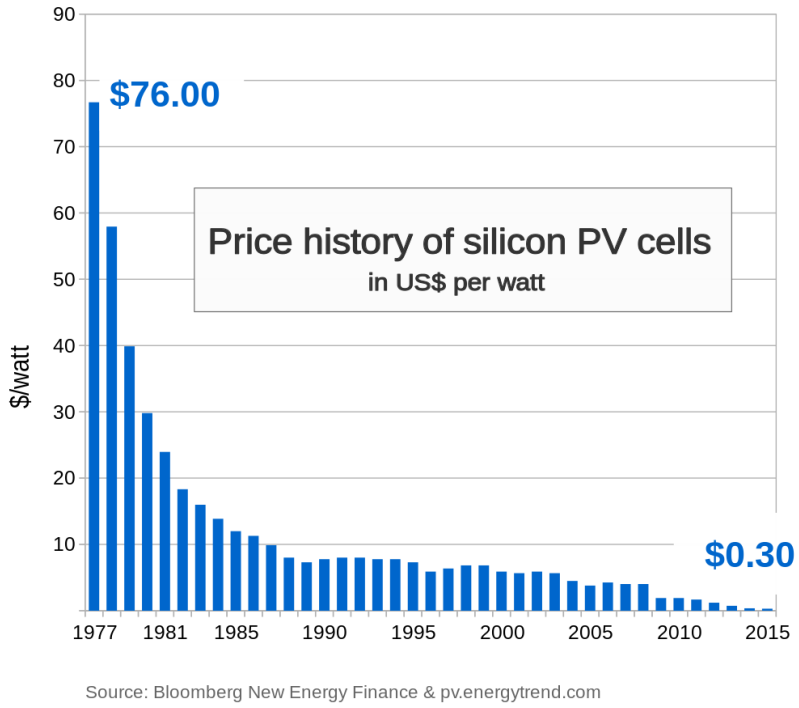

Figure 5: Price history of silicon PV cells

Since then, tremendous progress was made to make solar panels commercially available for the population. According to the National Renewable Energy Laboratory report in 2018, the price for price for solar energy is around $0.47 per watt:[6]

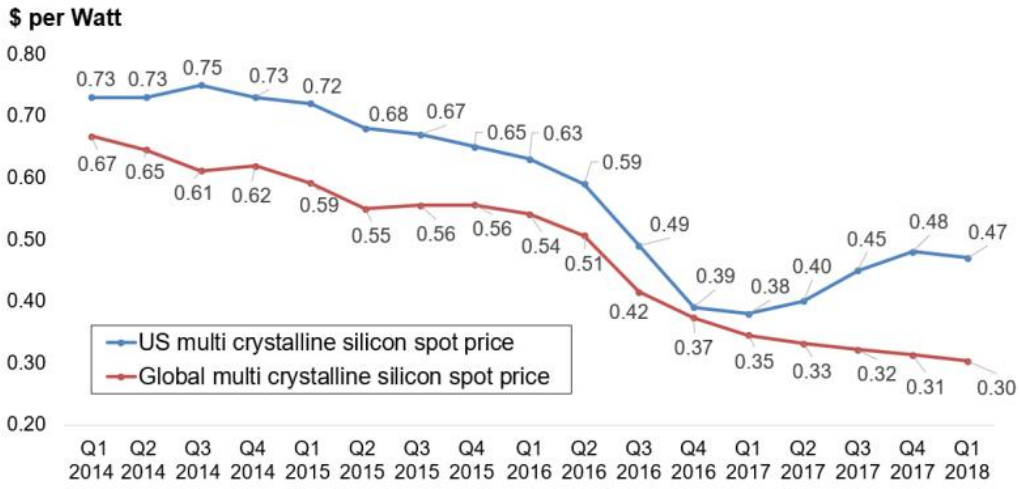

Figure 6: Spot price for crystalline silicon solar cell 2014-2018

2. Perovskite

2.1. History of perovskite

As silicon solar cells still dominate the field, attention is turning to perovskite semiconductors. Perovskite is a term used to describe a class of material with a crystal structure of ABX_3, where A is an organic cation, B is a metal cation, and X is a halide anion. As perovskite is only referring to the common structure of materials, there are many options for the application. For example, originally, most perovskite structures used oxygen as an anion, due to the fact that the first perovskite mineral that was discovered was $CaTiO_3$. However, due to its poor absorption, only 8 to 20% efficiency[7], the use of Oxygen as an anion was replaced with a halogen (e.g., Cl, Br, I). B element is almost always lead (Pb), there have been efforts to replace it to address the issue of lead effect on the environment, although still lacking in popularity. As of now, the most popular material for perovskite solar applications is methylammonium lead halide, by using methylammonium cation ($CH_3NH_3^+$), forming $CH_3NH_3PbI_3$. For the sake of simplicity, it was shortened into $MAPbI_3$ by many researchers. It has been used mainly as a photocatalyst for various applications, such as polymerization[8, 9] and CO_2 reduction[10]. It has also been used in the creation of efficient LEDs[11]. Perovskite is also known as a potent candidate in the photovoltaic field.

2.2. Perovskite solar cell structure

The base technology for perovskite photovoltaics solar cell is from dye-sensitized solar cells. Dye-sensitized solar cells operate with the same principle as the conventional silicon solar cell. The solar cell still forms the basic n-i-p blocks as normal. The only difference is that the dye is introduced as a separated light harvesting layer, instead of a depletion zone in silicon solar cell. In perovskite materials, both mesoporous structure and planar heterostructure are studied and developed and have different characteristics. In the early state of the field, planar heterostructure

had much lower efficiency than mesoporous structure[12, 13]. However, with intense research to improve the efficiency of planar heterostructure, it now has almost the same efficiency as the mesoporous structure[14, 15]. Factoring in mesoporous disadvantage of having a mesoporous TiO_2 scaffold that requires high temperature to manufactured, and its UV instability[16], heterostructure is preferable. That is not to say the mesoporous structure has not seen any improvement. Schulze et al. (2017)[17] developed a process in which the TiO_2 scaffold could be manufactured at low temperature, as well as improving its UV stability.

Although different in structure display, both show similar composition: A metal electrode layer (typically made of Au, Ag, Al)[18]; hole transport material (most commonly Spiro-OMeTAD (2,2′,7,7′-Tetrakis[N,N-di(4-methoxyphenyl)amino]-9,9′-spirobifluorene); an electron transport material (usually compacted TiO_2 or SnO_2)[19]; a layer of transparent conducting film, which is usually FTO/ITO; and a light-harvesting active layer, which is composed of only perovskite in the case of planar heterostructure case, or perovskite and a mesoporous oxide layer in the mesoporous structure case. Either way, each layer performs a similar function. When light travels to the perovskite layer, the photon within the light can knock an electron off the perovskite, creating holes and free electrons. Free charge carriers are then transferred to the hole and electron transport material, which acts as an n-junction and p-junction respectively. The metal electrode layer and FTO/ITO layer are used to connect the solar cell to the system that it is powering. Within the FTO/ITO layer, FTO is more popular than ITO due to its low and temperature-stable resistivity[20].

2.3. Strength of perovskite

2.3.1. Efficiency

While the perovskite PV solar cell only entered the competition in 2012, the field has evolved rapidly, with its current efficiency surpassing 20%[21].

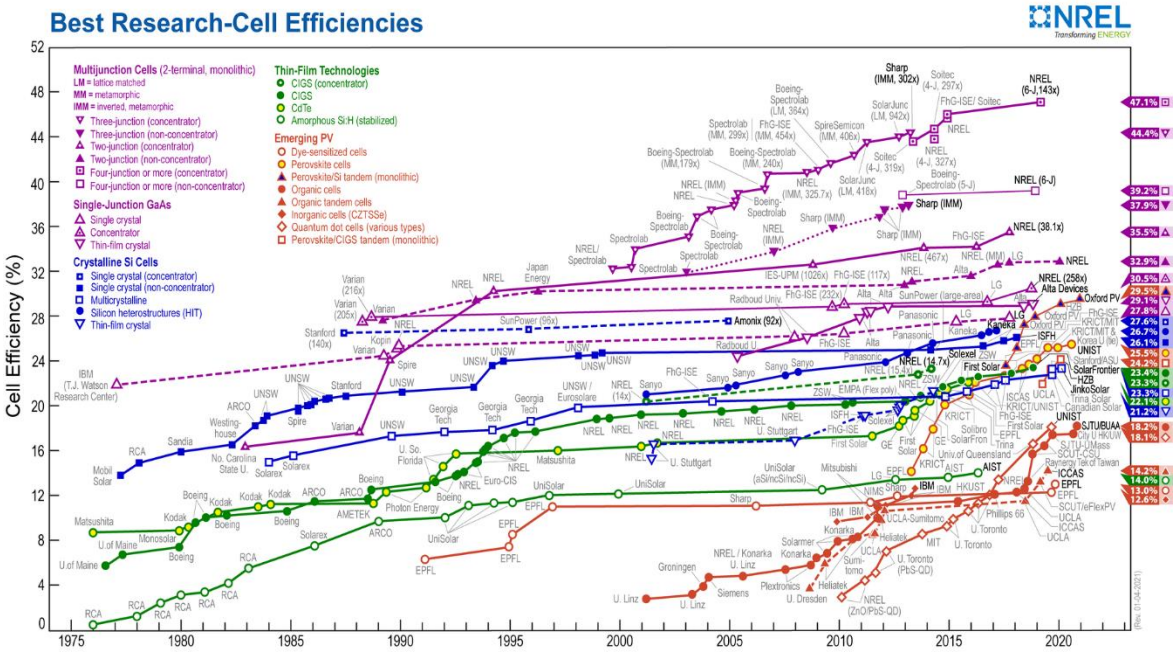

Figure 7: Reported timeline of research solar cell energy conversion efficiencies since 1976. Data obtained from National renewable energy laboratory (NREL), https://www.nrel.gov/pv/cell-efficiency.html.

Additionally, its Shockley–Queisser limit, which indicates the maximum theoretical efficiency of a single p-n junction, is around 33.7%, which indicates that there is still much room for development[4]. In comparison, that of the silicon solar cell is 26.7%[22]. Apart from using pure perovskite PV solar cells, it can be used alongside silicon to form a tandem device that could exceed 30% efficiency[23].

2.3.2. Manufacturability and thin-film nature

Besides its high energy conversion efficiency, another advantage of the perovskite PV solar cell lies in its manufacturability. For silicon solar panels, the material must go through a costly process to be manufactured[24]. Using its thin-film nature, perovskite can be fabricated using low-cost techniques, such as inkjet printing[25] or the roll-to-roll technique[26], thus enabling the material

to be mass-produced. Aside from its low manufacturing cost, the thin-film attribute also allows perovskite to be used in small devices, allowing more potential applications for the material. One such example is perovskite potential in manufacturing solar cell for smartphones.[27]

2.3.3. Tunable bandgap

Since perovskite is not preferring to one specific material, but a family of material, perovskite possesses the ability to tune its own bandgap. For example, as mentioned, the most popular perovskite material is $MAPbI_3$. However, in the situation where greater stability of the material is needed, the bandgap could be adjusted to a higher value. Doing so would limit the efficiency of the solar cell, since there is less usable sunlight, but increase the stability of the solar cell. The tunability of bandgap is done by replacing Iodine with other halide material, such as Bromine (Br) or Chlorine (Cl).[28, 29] This feature also allows many accommodation to fit many other specific requirements, such as efficiency, moisture requirements, etc. As mentioned, according to the Shockley-Queisser limit, the theoretical maximum efficiency of solar cell is achieved when the bandgap is about 1.4eV, while the minimum bandgap perovskite is able to achieved is around 1.48eV.[28]

2.4. Drawbacks and limitation

2.4.1. Losses

The loss in photovoltaic solar cell efficiency is composed of thermalization loss, below bandgap loss, optical loss, recombination loss and spatial relaxation loss[30, 31]. Overall, the loss mechanisms and the amount of loss in perovskite solar cells is summed up by Da et al. (2018)[30] with the following figures:

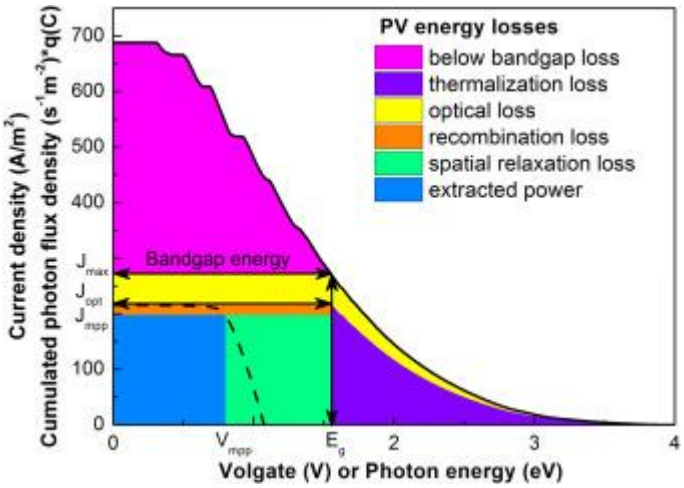

Figure 8: Energy loss occurring in the perovskite solar cells. Different colors represent different energy loss mechanisms[30]. Reprinted from Solar Energy Materials and Solar Cells, Vol 174, Yun Da, Yimin Xuan, Qiang Li, Quantifying energy losses in planar perovskite solar cell, 206-213, Copyright (2023), with permission from Elsevier.

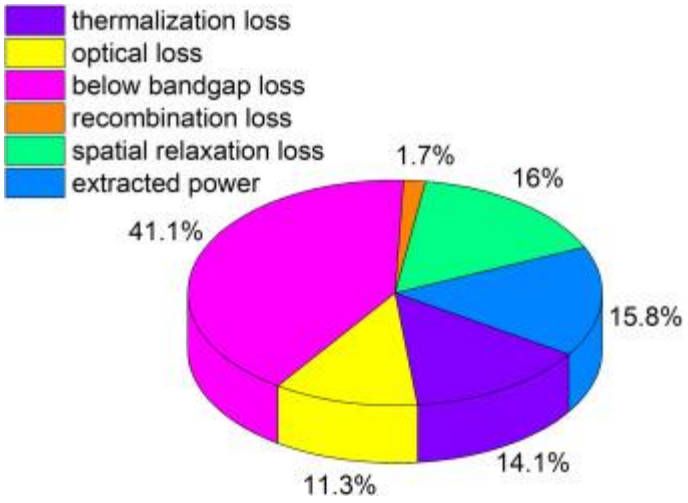

Figure 9: Quantification of energy loss occurring in the perovskite solar cells under AM1.5 illumination.[30]. Reprinted from Solar Energy Materials and Solar Cells, Vol 174, Yun Da, Yimin Xuan, Qiang Li, Quantifying energy losses in planar perovskite solar cell, 206-213, Copyright (2023), with permission from Elsevier.

2.4.1.1. Loss of below bandgap photons

Below bandgap loss occurs when the photon does not meet the energy criteria to excite the electron inside the material. These photons are simply lost and do not contribute to the solar cell. The most popular solution to this problem is simply lowering the bandgap of the material. Fortunately, this purpose aligns with the general direction of the perovskite field, given that in

order to achieve the Shockley-Queisser limit, a lower band gap is required, which will also reduce the below band gap loss by reducing its band gap.

2.4.1.2. Thermalization loss

As mentioned in an earlier section, when the solar cell is hit with a photon that carries higher energy than needed for the electron to cross the band gap, thermalization process occurs. In this process, the excess energy relaxes down to the band edge that is lost as heat (i.e., thermalization loss). In turn, the heat generated from this process causes the solar cell to heat up, which will cause it to degrade. In order to minimize this source of loss, an entire class of solar cell was developed, known as the "hot carrier solar cell".[32, 33]

Overall, these two types of losses (loss of below bandgap photons and thermalization loss) are the main losses of a photovoltaic solar application. These two losses combined account for over 50% of the total absorbed solar energy in solar. The trend is consistent across the photovoltaic field, as observed both in silicon and perovskite.[34]

Simply finding a different material does not solve the issue, as the two types (perovskite and silicon) have vastly different band gap value, yet the amount of loss remains the same. Therefore, although it could be agreed that the optimal band gap should follow the Shockley-Queisser limit, achieving this limit does not solve the trade-off, due to the two polar opposite nature. This implies that it would be best if a method could be used to minimize and/or harvest one of these two types of wasted energy specifically, without hindering the other.

2.4.1.3. Optical loss

Normally, when light hits the solar cell, some light normally would generate enough power to excite the electron, but unfortunately, it gets reflected. Optical loss also includes part of the light that never hits the solar cell. With the way that solar cells are organized, the metal electrode layers

need to be stacked on top of the light absorbing layer, which are represented as busbars and fingers. However, this also impedes the amount of active surface of the solar cell, thus limiting the amount of sunlight the solar panel received, called shading loss.[35] On the other hand, reducing the number of busbars and fingers will increase the resistance losses in the solar cell.[36] That is not to say that all the light that hit the perovskite layer got absorbed either, since a part of it would be transmitted through it, or being absorbed by other layers, which resulted in parasitic loss. There have been attempts to improve the loss of light getting transmitted through the perovskite layer called light trapping. The term light trapping is self-explanatory, it refers to trapping light inside the perovskite layer to improve its probability of the light being absorbed by the it.[37, 38]

2.4.1.4. Parasitic loss

Inevitably, the light trapping systems also have their own absorption rate, which adds in the parasitic loss. The light trapping system still proves to be beneficial to the solar cell, although the benefit is reduced by the effect of parasitic loss.[39] The material usually used for light trapping are Al and Ag nanoparticles, with Al nanoparticles display lower parasitic loss and is not as expensive as Al.[38, 40]

2.4.1.5. Recombination loss

Recombination loss occurs when the excited electron does not get collected and loses its energy. When this happens, the electron becomes stabilized and recombine with the hole. Fortunately, perovskite solar cells have long recombination lifetime,[41] so recombination loss is not a big issue.

2.4.1.6. Spatial relaxation loss

Spatial relaxation loss refers to the lost mechanism where the carriers lose their potential energy as they move along the band edge.[42]

2.4.2. Limitation

Perovskite solar cells stem from dye-sensitized solar cells. Therefore, they inherit some of their disadvantages: instability. This aspect is the main reason that perovskite is still not popularized as a solar cell material. There are two factors that lead to this instability issue: intrinsic instability and extrinsic instability.

2.4.2.1. Intrinsic instability

For intrinsic instability, the main factor is the fact that perovskites ions have relatively low activation energy, or "soft" interface.[43, 44] This means that the bonding of the crystal lattice is weak, leading to being easily interacted with the surrounding environment, leading to decomposition and interfere with other layers, mainly causing non-radiative recombination loss.

2.4.2.2. Extrinsic instability

Extrinsic factors come into play when the perovskite layer is exposed to the working environment, which includes temperature, moisture, and UV light.

2.4.2.2.1. Moisture

One of the leading aspects that cause this degradation process is moisture, which triggers the chemical reaction leading to material degradation.[45] To be more specific, with 98% relative humidity, the absorption of the material is dropped to half of its initial value with only 4h of exposure to the environment. In contrast, in the low relative humidity case (20%), the above degradation process would take up to 10000 h.[45]

2.4.2.2.2. UV light

Another reason for the degradation of the perovskite solar cell is due to UV light, or rather, the lack of UV light. A study had been conducted to measure the degradation of the electron

transport layer TiO_2 under different UV conditions. Surprisingly, encapsulated solar cell from UV light degrades the fastest among the cases involved in the study.[46]

2.4.2.2.3. Temperature

Temperature also plays a role in the degradation of the solar cell. The production process of the perovskite layer requires an annealing step, where it is required to go through elevated temperatures and eventually be exposed to high temperatures during operation[47, 48].Overall, the results from those experiments consistently show that the more heat is applied, the faster the cell degrades over time, although at different rates depending on the test conducted (in an N_2 environment, ultra-high pressure, etc.).

3. Singlet fission

3.1. Basic function

Among many attempts to address the thermalization loss[49-51], singlet fission could potentially minimize the thermalization loss and slow the heating process in a semiconductor.[52] Singlet fission is a process in which one singlet excited state electron is converted into two triplet state excitons.[53] In other words, singlet fission allows the absorption of photons with high energy, such as photons in the ultraviolet spectrum, and converts them into pair of excitons instead of one free electron. Figure 10 illustrates the basic function of singlet fission, while figure 11 shows how a singlet fission solar cell works:

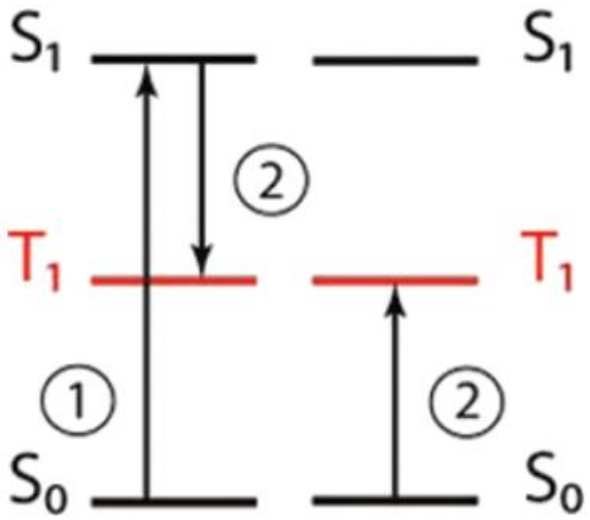

Figure 10: Singlet fission: (1) The chromophore on the left undergoes an initial excitation to S1. (2) The excited chromophore shares its energy with the chromophore on the right, creating a T1 state on each.[53]. Reprinted (adapted) with permission from Smith, M. B.; Michl, J. Singlet Fission. Chemical Reviews **2010**, 110 (11), 6891-6936.Copyright (2023) American Chemical Society.

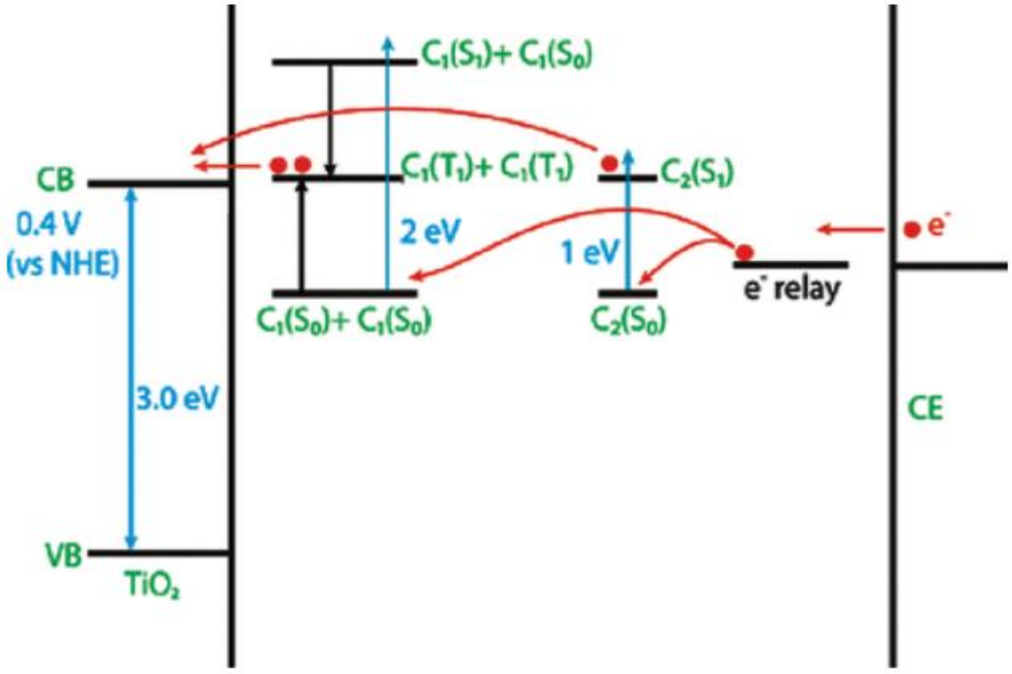

Figure 11: Dye-sensitized solar cell that uses a singlet fission sensitizer (C1) in conjunction with a conventional sensitizer (C2).[53]. Reprinted (adapted) with permission from Smith, M. B.; Michl, J. Singlet Fission. Chemical Reviews **2010**, 110 (11), 6891-6936.Copyright (2023) American Chemical Society.

Each exciton created by singlet fission would have less energy than a singlet state electron, reducing the thermalization loss mentioned above. Therefore, with the Shockley-Queisser limit being constructed with the thermalization loss accounted for, using singlet fission could potentially make the device's energy conversion efficiency surpass this limit, up to about 45% in the case of silicon solar cells.[54]

3.2. Effect on solar cells

Currently, singlet fission has been proposed for organic photovoltaic devices to improve photoconversion efficiency.[55] It is due its ability to convert the leftover energy in high energy photons, which would otherwise be wasted, into useable energy. Figure 12 compares the efficiency of singlet fission and a conventional dye-sensitized solar cell:

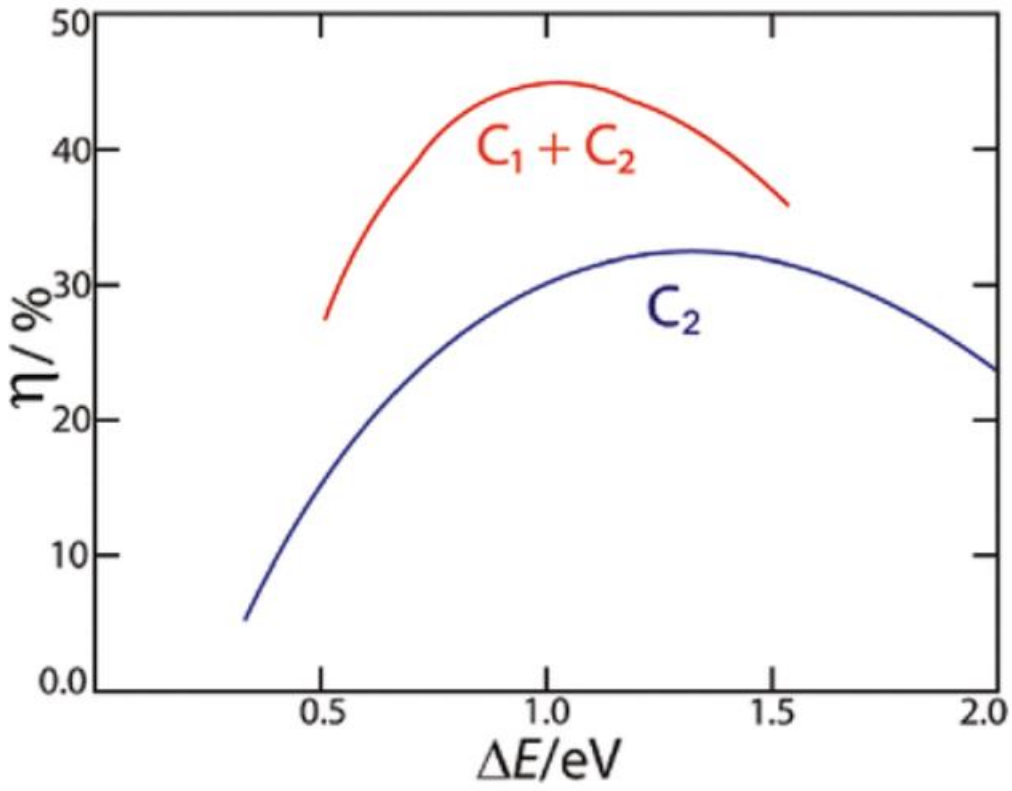

Figure 12: Schematic sketch of theoretical efficiency as a function of the S_0–T_1 band gap for a singlet fission solar cell and a conventional dye-sensitized solar cell.[53]. Reprinted (adapted) with permission from Smith, M. B.; Michl, J. Singlet Fission. Chemical Reviews **2010**, 110 (11), 6891-6936.Copyright (2023) American Chemical Society.

Recently, this singlet fission has been applied to silicon solar cells, using a material called tetracene.[56] Tetracene is a great material that fits the criteria for singlet fission but does not have a high enough band gap to completely match the requirement for an ideal coupled material for perovskite. This means triplet excitons produced by singlet fission could be lost. The debate regarding this issue is still ongoing.[57-59] Additionally, singlet fission does not result directly in free charge carriers, but triplet state excitons, which can undergo charge separation to become free charge carriers.[60] Moreover, D'Innocenzo et al. (2014)[61] show that the fraction of free charge carriers is correlated with temperature. This means the less heated the panel is, the fewer free

charge carriers are to be produced. Singlet fission would bring the inner temperature down due to the dissipation of heat generated from thermalization, effectively lowering the overall percentages of free charge carriers. In other words, applying singlet fission could potentially reduce its overall efficiency in exchange for stability. This downside could possibly be in the acceptable range since the need for stability in perovskite is much more urgent than its efficiency, as well as factoring in the boost in efficiency by applying singlet fission itself. As of now, the application for singlet fission in solar cells is limited. Singlet fission materials, namely pentacene, have seen use in silicon solar cells. However, most studies regarding this subject have been directed at boosting the efficiency of silicon. As for perovskite solar cells, there are limited resources for the effect of singlet fission on its efficiency and stability.

4. Study

This section relies mostly on a paper published by us.[62]

4.1. General overview

Perovskite materials suffer greatly from instability due to heat. The stability of perovskite materials is crucial for solar cell applications and its commercialization [47, 48, 63, 64].Much attention has been focused on improving perovskite stability, such as heat dissipation and material enhancements[49-51] .However, the potential benefit of heat transfer among layers within solar panels is often overlooked. Meanwhile, there have been developments in singlet fission in the photovoltaics field recently. These recent developments include the potential prospect of singlet fission in solar applications (Xia. et al., 2017)[65] and the internal quantum yield of tetracene-based organic solar cells (Wu. et al., 2014)[66]. Currently, most of the existing works only focus on the potential benefits of singlet fission to the conversion efficiency of a solar cell[56, 65, 66], while its effect on stability deserves more attention. This study offers new insights into the effects of singlet fission and heat transfer on perovskite solar cell stability by developing and investigating a new singlet fission/perovskite tandem solar cell model.

In this study, we suggested adding a layer of tetracene onto the perovskite layer to promote the process of singlet fission. We then examined the effectiveness of singlet fission on the perovskite photovoltaic device temperature by calculating the amount of thermalization loss between two cases: with and without singlet fission. We also modeled the heat transfer between the two cases to observe the effectiveness of coupling an extra layer of material on the temperature of the perovskite light-absorbing layer.

The study is separated into five parts to describe how the model was developed. In the first part, the general assumptions and the configuration setup used in this study were introduced. We designed two different cases to highlight the effect of coupling singlet fission materials on perovskite photovoltaics devices. The first case we evaluated was the control case, in which the solar cell without a singlet fission layer was added and simulated. After that, the tetracene case was evaluated, in which a layer of tetracene was coupled with the solar device to promote singlet fission.

Second, we modeled the incoming sunlight. This section is based on the work of Paulescu et al. in 2003.[67] Our objective in this section was to calculate the number of photons captured by the solar cell and the energy of each photon. Then, the energy of the photons was separated into components based on their energy compared to the bandgap of the material involved within each separate case. We also categorized photons into distinct groups that were used in other sections.

Third, the photon excitation process was modeled. In particular, the pathway that the photons took once they reached the solar panel is explained in this section. In this section, we described the control and tetracene case separately to show the difference in the pathway for the photons in each case. Furthermore, we also calculated the total amount of energy each layer absorbed and evaluated the amount of thermalization loss between the two cases.

Temperature is the main emphasis of the fourth section. In this part, two different heat generation/transfer methods were evaluated for each case. These were the thermalization heat generated from the excess energy of the photons, as well as the conductive heat transfer between layers within the solar cell.

Finally, the study evaluated the bandgap of the material. Here, we simulated how $CH_3NH_3PbI_3$ would change its material properties under the influence of heat. The temperature dependency of the bandgap is based on two factors: electron-phonon interactions and thermal expansion. The purpose of bandgap calculation was to determine the range of each classification of photons, which was explained in the second section. Our calculations are based on Francisco-López et al. in 2019[68] where the continuous change of bandgap was evaluated with respect to temperature.

4.2. Model Assumptions and Configurations

4.2.1. Model Assumptions

1. The sun intensity throughout the testing period was modeled as a constant.

2. The only environmental impact from the solar cell's working conditions considered was temperature. Other effects, such as moisture and dust, were not taken into consideration.

3. The perovskite material used in the study was $CH_3NH_3PbI_3$. The material used to promote singlet fission in this study was tetracene.

4. Thermalization loss was considered the only source of energy loss. Other sources, including parasitic loss and optical loss, were neglected due to the lack of generated thermal energy. The loss of non-absorbed photons was included to test the validity of the model.

5. The bandgap of the $CH_3NH_3PbI_3$ layer was modeled as a variable of temperature. However, due to the lack of research regarding the same topic with tetracene, their bandgaps were modeled as constant throughout the simulation.

4.2.2. Configuration

Figure 13 a and b describe the general setup of the two cases considered in this study, including the control case and the tetracene case if they were implemented in a conventional solar cell:

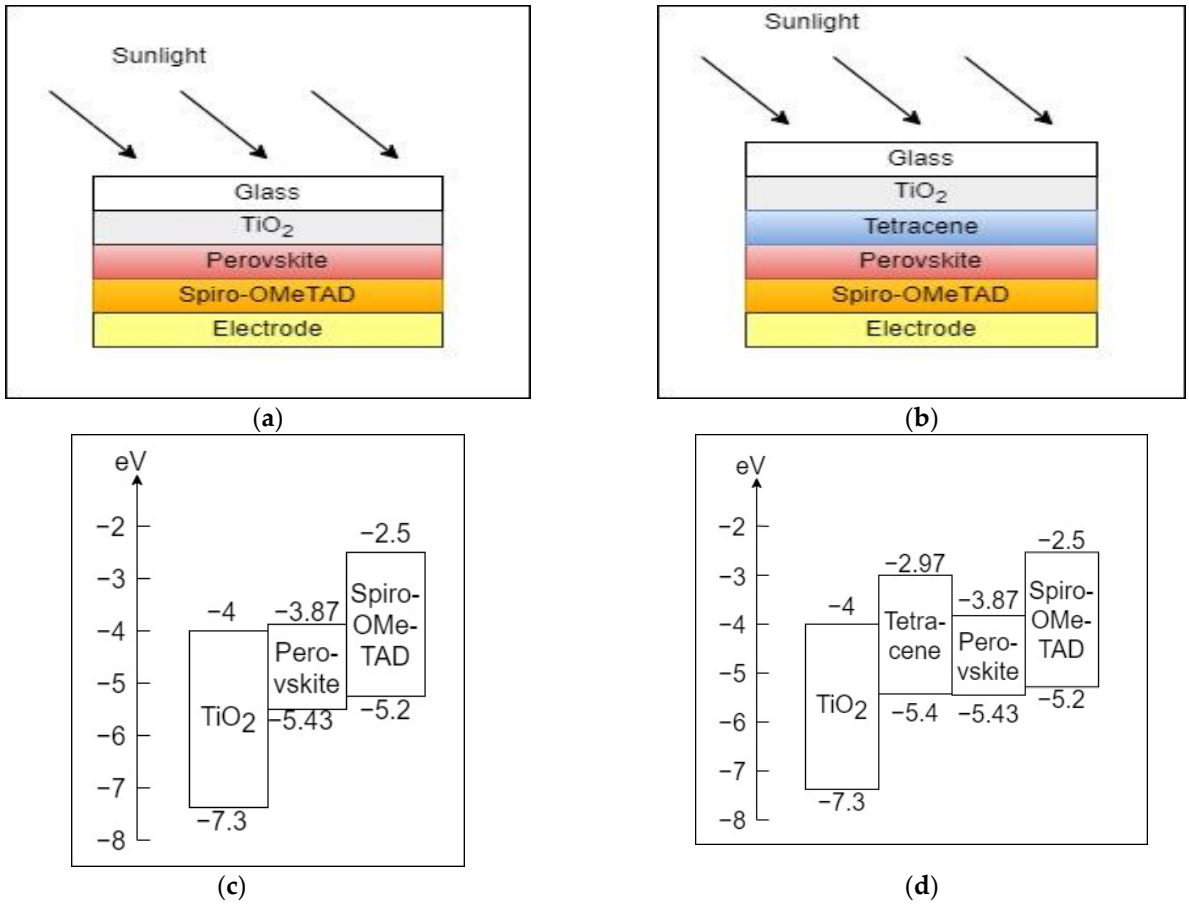

Figure 13: (a) The configuration for the control case. (b) The configuration for the tetracene case. (c) Band diagram for the control case. (d) Band diagram for the tetracene case.

The configuration setup of the control case is similar to the typical single junction n-i-p solar panel, with the TiO_2 layer acting as the anode layer; the perovskite layer as the main light absorber; and the Spiro-OMeTAD layer as the cathode layer. In the tetracene case, a layer of tetracene was added to promote singlet fission. By placing the tetracene layer directly above the

photon collecting layer, singlet fission could be performed effectively without interference with the main solar cell system.

Values for the band diagram were taken from Qin et al.[69] for TiO_2 and $MAPbI_3$; Nakka et al.[70] for Spiro-OMeTAD; and MacQueen et al.[56] for tetracene.

4.3. Incoming Sunlight Model

4.3.1. Solar Spectral Flux Density

Light plays a key role in solar cells. Not only does it provide the energy that will then be used by the solar cell to produce energy, but it is also one of the main causes of its degradation. This leads to difficulty in designing photovoltaic devices. The bandgap of semiconductors determines the energy required by photons to excite electrons in the light-absorbing layer to be conductive. Any photon with lower energy than the requirement is lost. However, simply reducing the bandgap of semiconductors is not necessarily beneficial for the device. When photons with higher energy than the bandgap energy hit the solar panel, the leftover energy is lost as heat, leading to the degradation of the material. This mechanism is referred to as thermalization loss. In the context of perovskite materials, the effect of thermalization loss is critical due to perovskite's inherent thermal instability. With this information, it is crucial to calculate how much light is available in terms of energy through the calculation of the solar spectral flux density.

The solar spectral flux density of the sun, assumed to be a black body with a temperature of 5762 K, can be approximated using Planck's law[71]:

$$G^0(\lambda) = \frac{10293\ \lambda^{-5}}{e^{\frac{2.5}{\lambda}} - 1} \tag{1}$$

where G^0 is the solar spectral flux density, and λ is the wavelength of photons.

Upon entering the atmosphere, a portion of sunlight is either reflected or refracted. This leads to the discrepancy between the spectral density flux at an extraterrestrial level and the amount of sunlight that reached the solar panel. To resolve this issue, Paulescu et al. (2003) made some adjustments to the original formula to account for those losses[67]. They are presented by the "a" term in the following equation:

$$a * \int_{0.2}^{4} G^0(\lambda) d\lambda = G_{SC} \tag{2}$$

where G^0 is the solar spectral flux density, and G_{SC} is the solar constant. In their work, the spectral density flux was equal to the solar constant, which was 1368 W/m^2, which led to the modification of its value to 0.809.

However, only using the solar constant would not provide more useful information about how much energy the application received, as the band gap of the solar photovoltaic devices is not continuous but quantized. This implies that every photon whose energy is below the bandgap energy would not excite electrons even though the combined energy of those photons could easily surpass the energy level of the said bandgap. On the other hand, the same effect could be said for when photons have more energy than the bandgap, in which case the electron in solar cells would only absorb enough energy to excite itself. The surmount energy will be lost as heat, as explained in the above thermalization loss definition. For these above reasons, the number of photons available for harvesting is needed, which is addressed in the following section.

4.3.2. Energy of Sunlight

The energy of a photon, simply denoted as E, was calculated using the following equation:

$$E(\lambda) = \frac{hc}{\lambda} \tag{3}$$

where h is the Planck's constant, c is the speed of light, and λ denotes the wavelength of the light.

To convert the number of photons existing in sunlight from solar spectral flux density, we use the following formula, with the applied adjusting parameter described above:

$$\phi(\lambda) = \frac{aG^0(\lambda)}{E(\lambda)} \tag{4}$$

where ϕ is the number of photons, G^0 represents the solar spectral flux density, and λ is the wavelength of photons.

This formula is straightforward, as it involves only dividing the total amount of energy within the spectral density flux, which is described in Section 4.3.1, by the energy of photons, as described by Equation (3).

4.3.3. Classification of Photons

For this simulation, there were three areas sunlight could be categorized into the following:

P_1: Photons with not enough energy to excite the CH3NH3PbI3 layer, with ϕ_1 photons in total.

P_2: Photons with enough energy to excite the CH3NH3PbI3 layer, but not enough to excite the singlet fission layer, with ϕ_2 photons in total.

P_3: Photons with enough energy to excite the tetracene layer, with ϕ_3 photons in total.

If the photon does not have enough energy to excite the electron in a layer, it would pass through that layer and onto the next. In particular, photons with class P_1 would neither be absorbed by the $CH_3NH_3PbI_3$ nor the tetracene layer. Meanwhile, photons with class P_2 would be absorbed by the $CH_3NH_3PbI_3$ layer, whereas photons with class P_3 would undergo singlet fission and generate two triplet state excitons, which would then be passed on to the $CH_3NH_3PbI_3$ layer for harvesting. The pathway of photons/electrons is explained below in Section 4.4. Ideally, P_3 should have an energy level twice as high as the energy level of P_2, which would result in the triplet state excitons generated from the singlet fission process possessing half the energy level from the original singlet state exciton. This would align perfectly with the requirements for the photon-absorbing layer bandgap. However, there are mismatches between the energy of singlet and triplet state excitons, which could hinder the efficiency of the singlet fission process.

The base bandgap of $CH_3NH_3PbI_3$ used in this study was 1.56 eV,[72] whereas tetracene's bandgap was only about 2.43 eV.[56] The base bandgap of tetracene leads to a triplet state excitons energy level of only 1.25 eV, which is lower than the bandgap of $CH_3NH_3PbI_3$.[69] When the energy level of the triplet state is lower than the bandgap of the photon-absorbing layer, the singlet fission process can still proceed efficiently.[56] This is due to the entropy net gain when producing two triplet excitons from one singlet exciton. However, the process is slower, giving rise to the potential of competing decay processes, notably singlet exciton transfer, triplet-triplet annihilation, and diffusion loss. As these decay processes are still under debate[58, 59, 65], they were not included in the simulation. In other words, the quantum yield of tetracene in this study was modeled as 200%, representing two triplet state excitons generated per photon absorbed. The triplet state excitons also ignored the energy mismatch and were modeled as having a compatible energy level with the photon absorber layer.

4.4. Modeling of the Pathways of Photons in Solar Cell

In this work, there were two types of simulations. The first one was the control case to demonstrate how the current solar cell model without the tetracene add-on would perform. The second simulation was the tetracene case, where a tetracene layer was added to evaluate its effect on the solar cell. The following subsections describe the inner mechanisms of a standard solar cell system, as well as the evaluation of the wasted energy generated in each case.

4.4.1. Photon Energy Component in Solar Cell

Upon excitation, the energy of a photon can be separated into components within the solar cell that satisfies:

$$E = E_g + E_w + E_b \tag{5}$$

where E is the total energy of the photon, E_g is the energy required to excite the electron within the material, and E_w is the wasted energy. Meanwhile, E_b is the binding energy. Note that the E_g and E_b values vary with different materials. It should also be noted that the bandgap value E_g is also temperature-dependent and was modeled accordingly in the study. Details about its dependency are explained in Section 4.6.

4.4.2. Control Case

Figure 14 describes the path that photons take in a normal perovskite solar cell. In this case, as described in Section 4.3.3, photons with enough energy, namely P_2 and P_3 class photons, are able to excite the grounded state electrons within the $CH_3NH_3PbI_3$ layer. Photons of class P_1 are not absorbed and passed through the $CH_3NH_3PbI_3$ layer, generating no energy in the process.

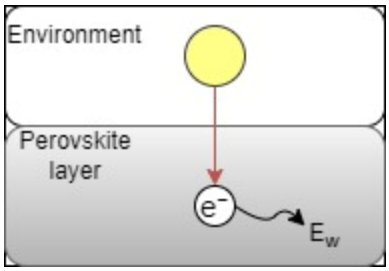

Figure 14: Pathway of photons into electrons in the control case.

The following equations describe the photon excitation process:

$$S_0 + E_{P_2} \rightarrow S_1 \quad (6)$$

$$S_0 + E + E_b \rightarrow S_1 + E_w \quad (7)$$

where S_0 denotes the ground electron state, and S_1 denotes the excited singlet state.

In the control case, the tetracene layer was not included. Thus, photons of class P_3 in this simulation function in the same manner as photons of class P_2. The amount of wasted energy was calculated using Equation (8):

$$\Sigma E_{w_{control}} = \left(\int_{\lambda_{P_2}}^{4} \phi E d\lambda \right) - E_{P_2}(\phi_2 + \phi_3) \quad (8)$$

The upper and lower bounds of the integration in Equation (8) were determined based on the frequency of the classification cutoff of each type of photon. In the control case, the lower boundary was set to be equal to the frequency corresponding to E_{P_2}, and the upper boundary was set to be 4 μm, where the amount of light reaching the solar panel reaches negligible levels.

4.4.3. Tetracene Case

Figure 15 illustrates the electron excitation process within different layers. Similar to the control case, photons with class P_1 pass through the two layers and are not absorbed. The P_2 photons pass through the tetracene layer effortlessly and reach the $CH_3NH_3PbI_3$ layer. On the other hand, P_3 photons are able to excite the singlet fission layer and produce two excited state electrons. The pathways for P_2 and P_3 photons are denoted by the dotted and solid lines, respectively.

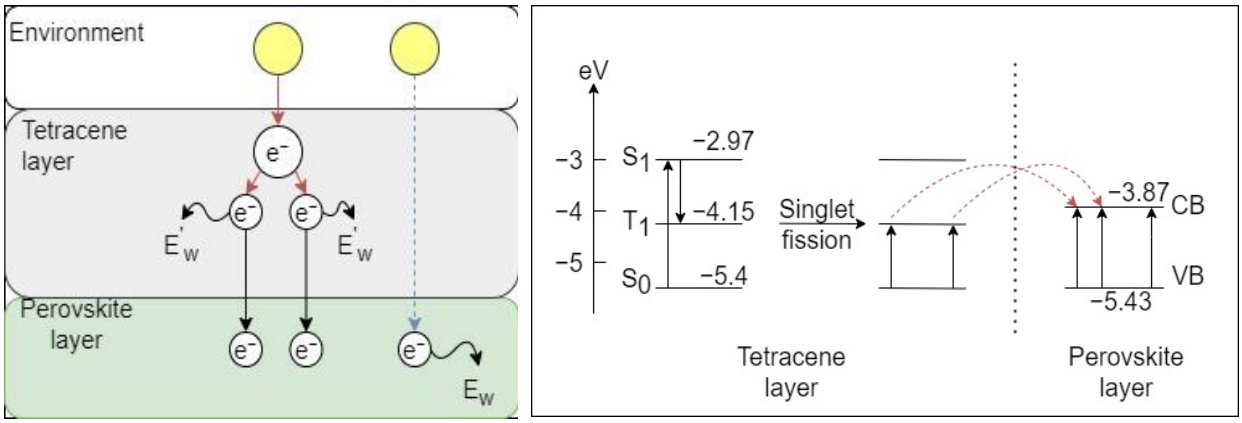

(a) (b)

Figure 15: (a) Pathways of photons into electrons in the tetracene case (b) Jablonski diagram for singlet fission in the tetracene case.

In the tetracene case, the first excitation does not happen in the $CH_3NH_3PbI_3$ layer but rather in the singlet fission sensitizer layer. In the singlet fission layer, the excited electron shares its leftover energy with its neighboring electron. Overall, the energy process within this case is detailed below:

$$S_0' + E_{P_3} \rightarrow 2R_1' \quad (9)$$

$$S_0' + E + E_b \rightarrow 2R_1' + E_W' \quad (10)$$

where S_0' denotes the ground electron state of singlet fission, while R_1' indicates the excited triplet state of the singlet fission layer. E_{P_3}'represents the energy required to excite the singlet fission layer. Lastly, E_W' represents the wasted energy from the singlet fission layer.

The amount of thermalization loss was calculated in the same manner as the control case:

$$\Sigma E_{w_{SF}} = \left(\int_{\lambda_{P_3}}^{4} \phi E d\lambda \right) - E_{P_3} \phi_3 \tag{11}$$

In the simulation, the tetracene layer was simulated to absorb all photons that have energy at least equal to the energy level E_{P_3}, the lower bound was set to be the frequency corresponding to E_{P_3}, and the upper bound was 4 μm.

The $CH_3NH_3PbI_3$ layer in this case was modeled to only receive the photons of class P_2. In this scenario, the amount of wasted energy in the $CH_3NH_3PbI_3$ layer was calculated using Equation (12):

$$\Sigma E_{w_P} = \left(\int_{\lambda_{P_2}}^{\lambda_{P_3}} \phi E d\lambda \right) - E_{P_2} \phi_2 \tag{12}$$

The lower bound in this case was set to be the frequency corresponding to E_{P_2}, and the upper bound was set to be the frequency corresponding to E_{P_3}.

The total amount of thermalization loss within the tetracene case is the sum of the two previous losses in Equations (11) and (12):

$$\Sigma E_{w_{SF}} = \Sigma E_{w_T} + \Sigma E_{w_P} \tag{13}$$

In order to evaluate the effect of singlet fission on the heating of the solar cell, a method to evaluate the solar cell's temperature with respect to time is needed. Here, we chose to calculate the temperature change based on two modes of heating: heating due to photon energy

thermalization loss and the conduction heat transfer between layers. We imposed a natural restriction: the cutoff temperature of the solar cell should be equal to 65°C. This restriction was made to reflect how heated the solar panel could be in summer. The effectiveness of the singlet fission mechanism was evaluated based on how fast the temperature rose with respect to time between the two cases considered in this study.

4.5. Modeling of Heat Transfer

In order to evaluate the effect of singlet fission on the heating of the solar cell, a method to evaluate the solar cell's temperature with respect to time is needed. Here, we chose to calculate the temperature change based on two modes of heating: heating due to photon energy thermalization loss and the conduction heat transfer between layers. We imposed a natural restriction: the cutoff temperature of the solar cell should be equal to 65°C. This restriction was made to reflect how heated the solar panel could be in summer. The effectiveness of the singlet fission mechanism was evaluated based on how fast the temperature rose with respect to time between the two cases considered in this study.

4.5.1. Heating Due to Photon Energy

As emphasized in previous sections, temperature plays a crucial role in this model. Formula (14) was used to describe the change of temperature based on the wasted energy calculated in Sections 4.4.2 and 4.4.3:

$$\Delta T_p = \frac{\Sigma E_w}{m\tau} \tag{14}$$

where ΣE_w is the wasted energy; m and τ indicate the mass and specific heat of the material. Lastly, ΔT_p represents the change in temperature due to photon energy.

The mass of the material is modeled as a constant throughout the simulation and was calculated using the parameters of a hypothetical solar panel size of 1 m by 1 m.

The bulk densities of $CH_3NH_3PbI_3$ and tetracene were 4.2864 g/cm^3 [73] and 1.2 g/cm^3,[74] respectively.

Normally, the specific heat symbol is c, but in this work, to avoid confusion with the speed of light, it was changed and denoted as τ instead.

The specific heats of tetracene and $CH_3NH_3PbI_3$ were based on the following literature[75, 76] and were found to be ≈1585 (J*kg^{-1}K^{-1}) for tetracene and ≈311 (J*kg^{-1}K^{-1}) for $CH_3NH_3PbI_3$.

4.5.2. Heating Due to Heat Transfer

4.5.2.1. Overall

Since the solar cell is made up from multiple layers, it requires massive computational time to solve it layer by layer. Therefore, we employed similar process to Lopez-Varo et.al[77] to find the temperature of the layers for each time step. In their work, the overall equation is:

$$C_i' \frac{dT_i}{dt} = G_{cd,i,j}(T_j - T_i) + G_{cv,i,a}(T_a - T_i) + G_{r,i,sky}(T_{sky} - T_i) + G_{r,i,gro}(T_{gro} - T_i) + (\phi S_i) \quad (15)$$

$$C_i' = \rho_i S_i d_i C_i \quad (16)$$

where G terms are the equivalent thermal exchange coefficient between layers. ρ, S, d, C, C' denotes the density, surface area, thickness, thermal capacitance, and capacitive contribution of the layer. The ϕS_i term refers to the thermal energy absorbed by the layer, reminiscing the thermalization energy from our work. The subscript cd, cv, r, a, sky, gro denote conduction, convection, radiation, ambient, sky, and ground, respectively. Using this overall equation, we can directly find the amount of heating toward the outer layer in one step.

4.5.2.1.1. Conduction

For conduction heat transfer, the equivalent thermal exchange coefficient is:

$$G_{cd,i,j} = \frac{1}{\sum \frac{d_i}{S_i * \gamma_i}} \tag{17}$$

where γ denotes the thermal conductivity of the layer.

4.5.2.1.2. Convection heat transfer

The convective component is only significant in the front and back glass is governed by the following equations:

$$G_{cv} = h_{conv} v_w S \tag{18}$$

$$(h_{conv,FG})^3 = \left(h_{free}\right)^3 + \left(h_{forced}\right)^3 \tag{19}$$

$$(h_{conv,BG})^3 = \left(h_{free}\right)^3 \tag{20}$$

$$h_{free} = 1.31\left(T_{FG,BG} - T_a\right)^{\frac{1}{3}} \tag{21}$$

where v_w is the wind velocity; T_a is the ambient temperature; h_{free} is the free convection; h_{forced} is the forced convection. $T_{FG,BG}$ is either the temperature of the front or back glass, depending on the layer being analyzed. As many values are dependent on the location/time of day, in our work, it is chosen arbitrary for simplicity. As such, v_w was set to be 0.5m/s; $T_a = 25°C = 298.15K$; $h_{forced} = 5.7$.

4.5.2.1.3. Radiation heat transfer

The radiation heat transfer mechanism in the front and back glass are governed by the following set of equations:

$$G_{r,i,gro} = \varepsilon_g F_{i,gro}\sigma(T_i + T_{gro})(T_i^2 + T_{gro}^2) \quad (22)$$

$$G_{r,i,sky} = \varepsilon_g F_{i,sky}\sigma(T_i + T_{sky})(T_i^2 + T_{sky}^2) \quad (23)$$

$$F_{FG,sky} = \frac{1}{2}(1 + \cos(\beta)) \quad (24)$$

$$F_{FG,gro} = \frac{1}{2}(1 - \cos(\beta)) \quad (25)$$

$$F_{BG,sky} = \frac{1}{2}(1 + \cos(\pi - \beta)) \quad (26)$$

$$F_{BG,gro} = \frac{1}{2}(1 - \cos(\pi - \beta)) \quad (27)$$

$$T_{sky} = 0.0552 T_a^{1.5} \quad (28)$$

where ε_g is the emissitivity of the glass; F_i are the configuration factors; T_{sky} is the temperature of the sky; β is inclination; σ is the Stefan-Boltzmann's constant. The ε_g value is 0.88, while the β value is set to be $\frac{\pi}{4}$.

4.5.2.2. Control case vs tetracene case

In the control case, the process could be evaluated using the equations presented by Lopez-Varo et.al[77]. However, in the tetracene case, the process is more complicated. In the tetracene case, the tetracene also contributes to the initial thermalization heating. Therefore, to simplify our equations, we simulated that the first conduction heat transfer occurs between the tetracene and perovskite layer only. After the first heat transfer step, the tetracene and perovskite layer are "merged" into a composite layer.

The first conduction heat transfer in the tetracene case is described by the following equation:

$$Q_{pev} = m_{pev}C_{pev}(T_{pev} - T') = m_{tet}C_{tet}(T' - T_{tet}) = Q_{tet} \quad (29)$$

$$T' = \frac{C'_{pev}T_{pev} + C'_{tet}T_{tet}}{C'_{pev} + C'_{tet}} \quad (30)$$

where m is the mass of the layer; C is the specific heat of the material; $T'$is the temperature of the two layers after the heat transfer. The subscript pev and tet denotes the perovskite and tetracene layer respectively.

For the composite layer, the C'_{comp} term can be related to C'_{pev} and C'_{tet} by solving the following equation:

$$Q = C'_{comp}(T' - T) = C'_{pev}\left(T_{pev} - T\right) + C'_{tet}(T_{tet} - T) \tag{31}$$

where T is the initial temperature of the layers, while T_{pev} and T_{tet} denotes the temperature of the perovskite and tetracene after the thermalization process occurred. Solving equation (31) with T' from equation (30) yields:

$$C'_{comp} = C'_{pev} + C'_{tet} \tag{32}$$

After replacing the perovskite and tetracene layer with the composite layer, equation (15) through (28) is evaluated as the control case.

4.6. Modeling of the Bandgap

As the temperature changes, the bandgap of $CH_3NH_3PbI_3$ also changes accordingly. This change affects the criteria for the classification of photons in Section 4.3.3 and, subsequently, Equations (8)–(13). The change in bandgap is due to two factors: thermal expansion and electron-phonon interaction. These factors, as well as how to derive them, were summed up by Francisco-López et al. in the following equations:[68]

$$\frac{dE_g}{dT} = \left[\frac{dE_g}{dT}\right]_{TE} + \left[\frac{dE_g}{dT}\right]_{EP} \tag{33}$$

where $\frac{dE_g}{dT}$ is the change of bandgap with respect to temperature. $[\frac{dE_g}{dT}]_{TE}$ and $[\frac{dE_g}{dT}]_{EP}$ represent the change of bandgap due to thermal expansion and electron-phonon interactions, respectively.

4.6.1. Change of Bandgap Due to Thermal Expansion

The change of bandgap due to thermal expansion is because of the contraction of the lattice with the decreasing temperature and was calculated by Equation (20):

$$[\frac{dE_g}{dT}]_{TE} = -\alpha_V B_0 \frac{dE_g}{dP} \tag{34}$$

where $[\frac{dE_g}{dT}]_{TE}$ denotes the change of bandgap due to thermal expansion. α_V is the volumetric expansion coefficient, while B_0 represents the bulk modulus. Meanwhile, $\frac{dE_g}{dP}$ signifies the change of bandgap with respect to pressure. The values for these parameters were summarized by Francisco-López et al. to be $\alpha_V = 1.57 \times 10^{-4}$ K^{-1}; $B_0 = 18.8$ Gpa; and $\frac{dE_g}{dP} = -50$ $\frac{meV}{GPa}$.

4.6.2. Change of Bandgap Due to Electron-Phonon Interactions

The change of bandgap due to electron-phonon expansion includes the Debye–Waller and self-energy corrections and was calculated by:

$$[\frac{dE_g}{dT}]_{EP} = \frac{A_{eff}}{4T} \frac{\hbar\omega_{\text{eff}}}{k_B T} \frac{1}{sinh^2(\frac{\hbar\omega_{\text{eff}}}{2k_B T})} \tag{35}$$

where $[\frac{dE_g}{dT}]_{EP}$ is the change of bandgap due to electron-phonon interactions; A_{eff} represents the electron-phonon coupling constant; $\hbar\omega_{eff}$ denotes the average phonon frequency; and k_B is the Boltzmann constant. The values for these parameters once again were presented by Francisco-López et al. to be A_{eff} = 8.09 meV and $\hbar\omega_{\text{eff}}$ = 5.87 meV.

After calculating the resulting bandgap, Sections 4.4 through 4.6 were repeated with the updated values to evaluate the next time step.

4.7. List of properties

Table 1 lists the set of material properties used in the study:

Table 1: Properties of materials

	Perovskite	**Tetracene**	**Glass**	**TiO_2**	**Spiro-OMeTAD**
Density (kg/m^3)	4286.4 [73]	1200 [74]	2400 [78]	4250 [78]	1020
Specific heat capacitance ($J*kg^{-1}K^{-1}$)	311 [75]	1585 [76]	800 [78]	-	-
Thermal conductivity (W/Km)	0.3 [79]	0.16 [76]	1 [78]	8.8 [78]	0.1 [80]
Surface area (m^2)	1	1	1	1	1
Thickness (nm)	Varies	Varies	10^6	190	360
Bandgap (eV)	Varies	2.43 [56]	-	-	-
Binding energy (meV)	50 [81]	-	-	-	-
Cutoff temperature (K)	338.15	338.15	338.15	338.15	338.15
Base temperature (K)	300	300	300	300	300

4.8. Model Implementation

Figure 16 showcases the flowchart detailing the sequence in which the study is carried out. The process encompasses both the control case and the tetracene case:

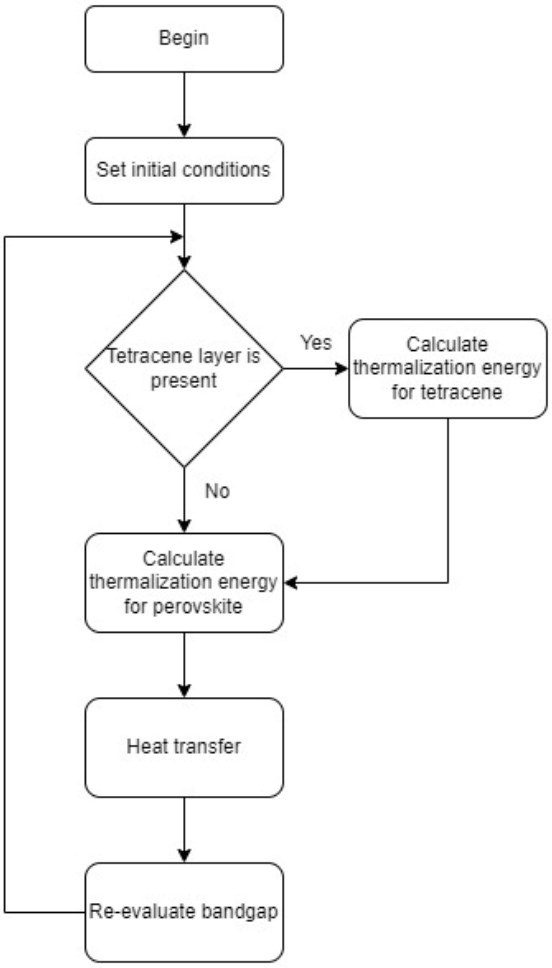

Figure 16: Flowchart for the study with the control and tetracene case

Overall, the processes for the two cases are mostly identical. The only difference between them is the present of the tetracene layer. If the tetracene layer is presented, i.e tetracene case, the model will evaluate the thermalization energy for both the tetracene and perovskite layer. After calculating the thermalization energy, heat transfer is performed to calculate the temperature of the material for the next timestep. The bandgap is also re-evaluated based on the new temperature. After that, the next timestep is evaluated. This cycle will be repeated until the end of the simulation.

4.9. Model Validation and Calibration

4.9.1. Model Validation

To test the validity of the model, two sets of data were employed. The first set of data follows the work of Hirst et al. (2010),[82] while the second was generated in this study. The reason Hirst's study was chosen is because their work provided us with all the necessary data while remaining straightforward and easy for us to reproduce. Their work also provided the best fit for our data and generally agreed with many other sources, such as Heidarzadeh et al. (2020)[34] and Da et al. (2018).[30] The fraction of loss due to the non-absorption of below-bandgap photons and thermalization were calculated in two studies were compared. The following equations were used to calculate the two variables in this study:

$$\%E_{below} = \frac{\int_{0.2}^{\lambda_P} \phi(\lambda)E(\lambda)d\lambda}{\int_{0.2}^{4} \phi(\lambda)E(\lambda)d\lambda} \tag{36}$$

$$\%E_w = \frac{\Sigma E_w}{\int_{0.2}^{4} \phi(\lambda)E(\lambda)d\lambda} \tag{37}$$

The ΣE_w value in Equation (36) follows Equation (8) closely, only varying in the λ_P value. Equations (36) and (37) were then tested with different bandgap values by varying λ_P and, subsequentially, ΣE_w to test its consistency with other literature.

4.9.2. Model Validation Result

Figure 17 shows the results of the comparison. It is clear that our method closely follows Hirst et al. (2010)'s work. These results also agree with other literature [27,61]. Table 2 shows the maximum errors, as well as the bandgap value of said errors between the two sets of data.

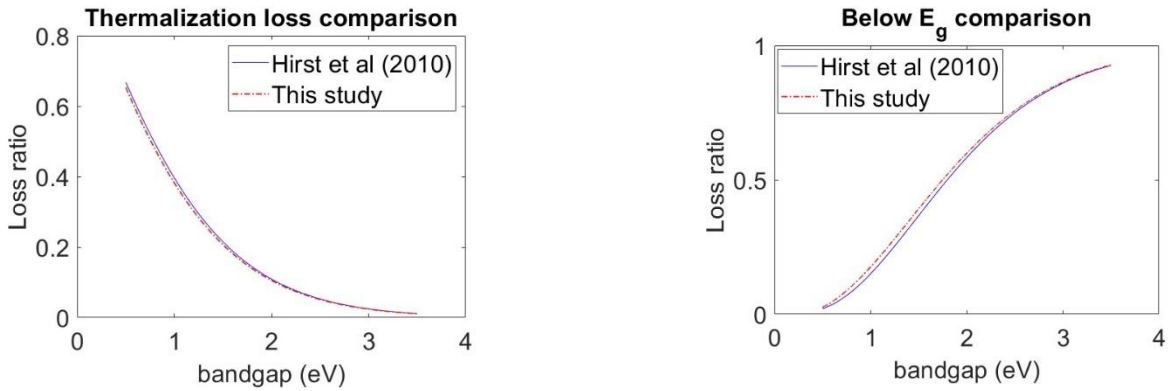

(a) (b)

Figure 17: Comparison of loss due to (a) Thermalization and (b) Below E_g between this study and Hirst et al. (2010)[74]

Table 2: Maximum absolute error in loss calculations and their corresponding bandgap values

	Thermalization	**Below E_g**
Maximum absolute error	0.0162%	0.0277%
Bandgap value	1.225 eV	0.713 eV

In this study, four tests were performed. The first test was used to examine the initial effect of the tetracene layer on the de-heating of the perovskite layer. The value for the perovskite layer was chosen to be 400×10^{-9} m or 400 nm. This reflects the average thickness of the perovskite layer in a conventional solar cell. The thickness of the tetracene layer was arbitrarily chosen to be the same as the thickness of the perovskite layer, i.e., $400\ nm$. The optimum value for the tetracene thickness will be examined and discussed in a later test.

In the second test, different thicknesses of the two layers were examined. This test served to establish the trend when different thicknesses of the two layers were applied. The reference values were chosen arbitrarily and were chosen to be twice the value in the reference case. The test was compared to the base condition to establish said trends.

In the third test, the optimum value for the tetracene thickness was investigated. The test was conducted by setting different values for L_{tet} and examined the temperature of the tetracene layer after an instant of time.

4.10. Results and Discussion

4.10.1. Effect of Singlet Fission on Losses

Figure 18 and Table 3 display the percentage of loss due to thermalization and below-bandgap photons in the perovskite layer in the control and the tetracene case. It is easy to see that adding a layer of tetracene into the system dramatically decreases the thermalization loss of the perovskite layer. More specifically, with the same amount of input energy, the percentage loss due to thermalization drops to 5.36%, compared to 17.95% in the control case. Moreover, since the difference in thermalization loss between the two cases was converted into triplet state excitons by singlet fission, the reduced amount can contribute to the efficiency of the solar cell. Meanwhile, the tetracene layer did not contribute to the mitigation of below-bandgap photons. Therefore, the percentage loss remains identical to the control case, at 43.55%. This makes sense, given that singlet fission only occurs when the photon energy is higher than the bandgap of the tetracene layer, which is higher than the bandgap of perovskite. With these data, we could conclude that coupling a tetracene layer to the perovskite solar cell system is able to convert thermalization loss into usable electrons, while not increasing the E_g loss. Therefore, we could draw the inference that the tetracene layer could potentially increase the efficiency of the solar cell system.

As mentioned in earlier sections, the mismatch in bandgaps of the two materials and their effect on singlet fission is under debate and is neglected here, although it could be the focus of a future study.

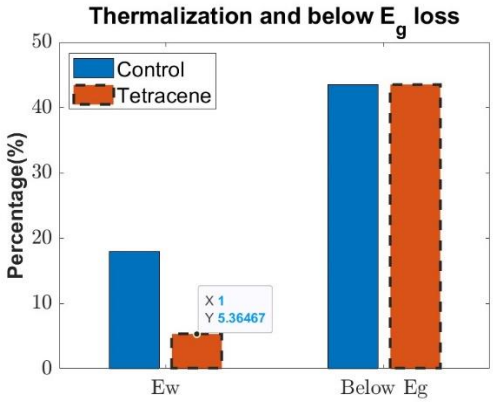

Figure 18: Amount of loss due to thermalization loss and loss due to below-bandgap photons in the perovskite layer between the control case and the tetracene case.

Table 3: Thermalization and below E_g loss between the control and tetracene case.

	Thermalization	Below $\boldsymbol{E_g}$
Control	17.95%	43.55%
Tetracene	5.36%	43.55%

4.10.2. Effect of Singlet Fission on the Heating of the Perovskite Layer

Figure 19 describes the temperature of the perovskite layer between the control case and the tetracene case. In the control case, simulated solar cell works similarly to a conventional solar cell. That is, perovskite layer generates thermalization energy, and subsequently, heat and raises the temperature of the solar cell to equilibrium temperature. One note-worthy detail is that, in the simulation, the solar cell in the control case reached equilibrium around 300.5K, instead of reaching the cutoff temperature. This is due to the fact that the environment temperature T_a is modeled as a constant. In reality, T_a is dependent on the location, time of day, as well as the heat transfer with the solar cell. However, in this study, it was modeled as a constant at 300K. In contrast, the tetracene layer successfully reduced the heat generated, allowing other heat dissipation mechanisms, such as convection and radiation heat transfer between the glass layers

and the environment. Therefore, the temperature of the solar cell remains almost unchanged throughout the simulation.

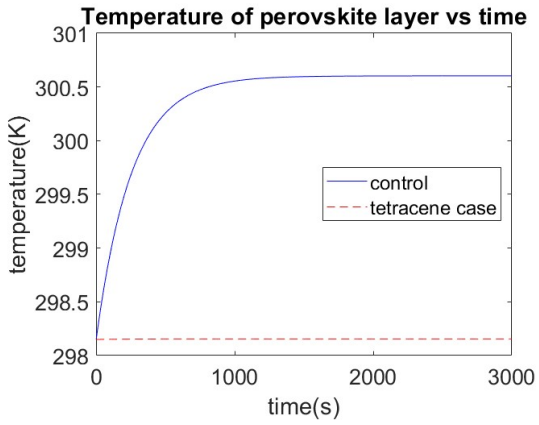

Figure 19: Temperature of the perovskite layers

In order to observe the effect of singlet fission more directly, we also simulated the control and tetracene case without any other heat dissipation mechanisms. The result is displayed in Figure 20. We can clearly see that without the tetracene layer, the perovskite layer reaches the cutoff temperature more rapidly, at around 20s. In contrast, the perovskite layer coupled with the tetracene layer only reaches the cutoff temperature at 100s.

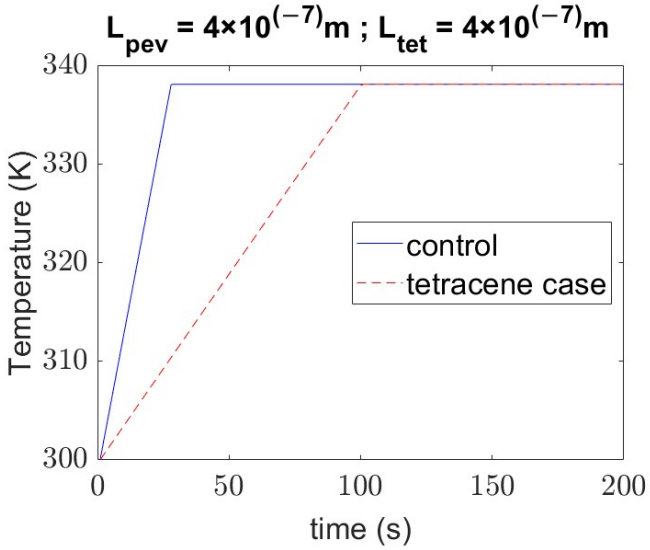

Figure 20: Temperature of the perovskite layer with the base conditions in isolation.

4.10.3. Effect of Varying the Thickness of Materials on Temperature

The thickness of the layers plays an important role in the temperature of the layers. If the thickness of the tetracene layer was set to be too low, the heating of the tetracene layer would be quicker than the perovskite layer. This could potentially cause the perovskite layer to degrade even faster due to the heat flux coming from the tetracene layer.

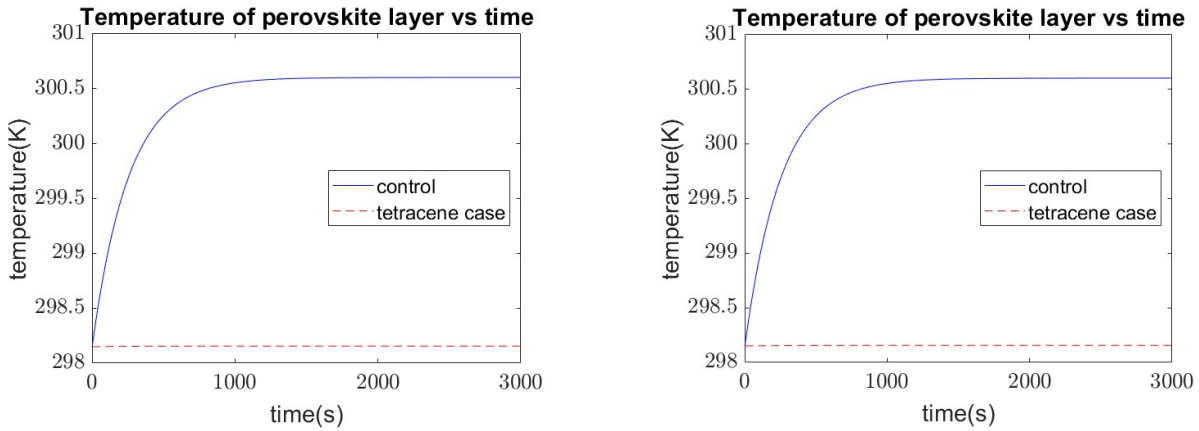

(a) (b)

Figure 20: Temperature of the perovskite layer when (a) the thickness of the perovskite layer is 800nm (b) the thickness of the tetracene layer is 800nm.

Overall, adjusting the thickness of the layers does not affect the result of the simulation much, except for the slight slower rise in temperature for the thicker perovskite layer case. Once again, to observe the effect of singlet fission more directly, Figure 22 displays the temperature of the perovskite layer when other heat dissipation mechanisms are not involved:

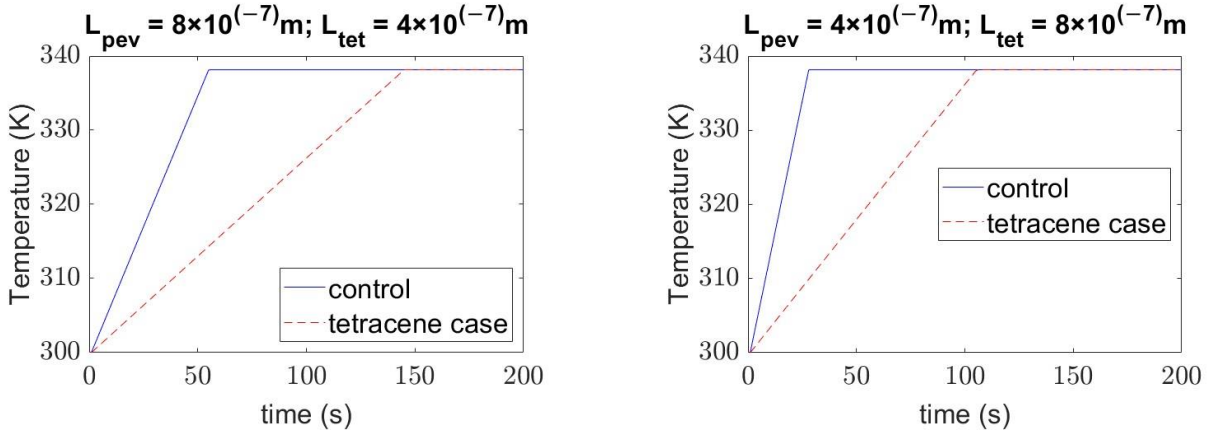

(a) (b)

Figure 21: Temperature of the perovskite layer in the control and tetracene case in isolation with a) The thickness of the perovskite layer is twice the reference value b) The thickness of the tetracene layer is twice the reference value.

By examining Figure 22a, it is clear to see that increasing the thickness of the perovskite layer results in a slower slope in both cases. This result is reasonable, given that the perovskite

layer exists in both cases. Moreover, comparing this figure with Figure 6, we can see that the change in thickness of the perovskite layer benefits the tetracene case more. In the control case, the time to reach the cutoff temperature is about 50s, as opposed to 20 s in the base condition. On the other hand, in the tetracene case, the change is around 50s compared to the base condition. However, given that one of the main advantages of perovskite solar cells is its thin-film nature, increasing its thickness is not always the ideal solution.

On the other hand, Figure 22b suggests that increasing the thickness of the tetracene layer benefits the tetracene case exclusively. This is due to the fact that the tetracene layer only exists in the tetracene case. However, the change is much smaller compared to increasing the perovskite layer, with the difference in time only being about 2s. From the data from Figure 22b, we could draw the conclusion that if the tetracene layer is thin enough, the tetracene system could be detrimental to the perovskite layer instead of helping it. Figure 22 shows the case in such a scenario, where the tetracene's thickness was set to be much lower than the thickness of the perovskite layer. In Figure 23, we can clearly see that the perovskite layer in the tetracene case reaches the cutoff temperature almost instantly, while the control case remains unchanged compared to the base conditions, further confirming our trend.

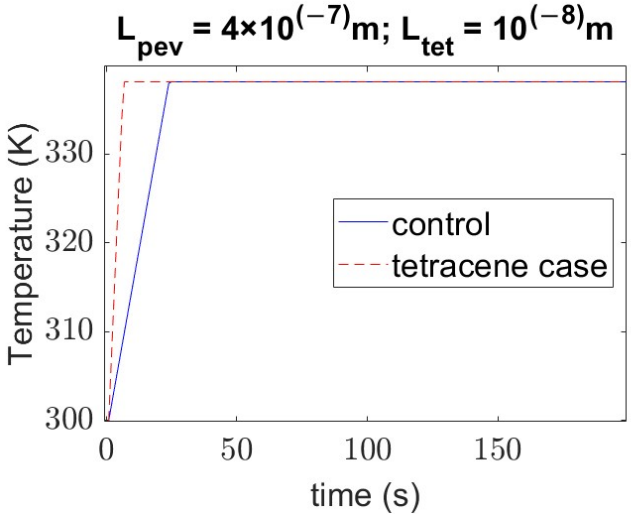

Figure 22: The control and tetracene temperature of the perovskite layer in the case of a thin tetracene layer.

Figure 24 displays the temperature after the initial heat transfer at the boundary layer between the perovskite and tetracene layer as a function of the thickness of the tetracene layer. The perovskite thickness was set as 400×10^{-9} m in this figure. As the figure shows, the perovskite layer in the control case does not change its temperature value with varying thicknesses. This makes sense since the tetracene layer is not involved in the control case. Meanwhile, we can see that with the tetracene thickness being close to zero, the temperatures of both the tetracene and perovskite layer in the tetracene case are higher than the value in the control case. The reason for such results is due to the heating of the tetracene layer. In the tetracene case, the temperature in the tetracene layer rises faster than in the perovskite layer. In other words, heat transfer is a detriment to the perovskite layer if singlet fission is implemented. In the case of thin tetracene layers, the cost of heat transfer outweighs the benefits of thermalization reduction. However, in the case of thick tetracene, such a cost is mitigated, leading to a reduction in the temperature of the perovskite layer.

Figure 24 also confirms that increasing the thickness of the tetracene layer is beneficial to the de-heating process in the perovskite layer. However, once again, with the strength of perovskite solar cells being their thin-film nature, the solution is not as straightforward as just increasing the thickness of the layer. In order to design a solar cell utilizing singlet fission while retaining its thin-film nature, the thickness of layers should be taken into consideration. Using data from Figure 24, we can conclude that the optimum value for the tetracene layer is around 1.75×10^{-8} m.

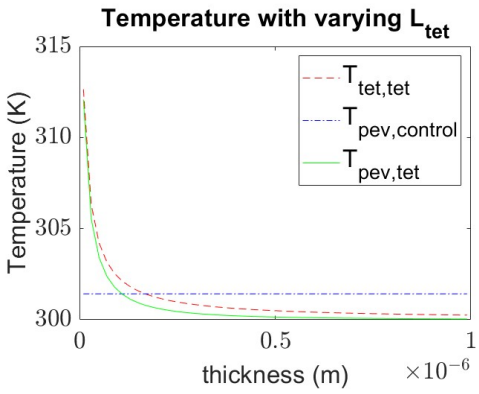

Figure 23: The temperature after the first timestep for each layer with respect to various tetracene layer thickness.

Conclusion and recommendation

This study presented a model investigating the amount of loss by a perovskite solar layer with and without singlet fission. This model closely follows other similar literature while remaining simple and efficient. We also developed a simulation to show the rate of increasing temperature in the perovskite layer. Two simulations were performed to compare the rate of increasing temperature in the control setting and the tetracene setting. Our results show that coupling singlet fission provided a significant benefit to the overall temperature of the solar cell. Through documenting the thermalization and loss of below-bandgap photons of the control and tetracene case, our study shows that coupling a layer of tetracene provides a potential benefit to the efficiency of the perovskite solar cell. Our study also shows that coupling an appropriate layer of tetracene will slow the temperature rise in the perovskite layer, providing time for other heat dissipation modes to take effect and effectively reducing the operating temperature of the solar cell. In the long run, this will help the long-term health of the solar cell. This study also implies another significant aspect that can contribute to the longevity of perovskite life expectancy. By coupling another material, in this case tetracene, conduction heat transfer is introduced into the system, contributing to the de-heating effort of the material. This opens the implication to dive deeper into the effect of other mechanisms to perovskite lifespan, such as the perovskite-silicon tandem cell. As the writing of this paper, the effort of such system is usually focused on the advantage on efficiency, with little attention to material stability. This paper may help with solidifying the benefit of such a system. Aside from that, this paper also highlights a meaningful parameter when designing a tandem solar cell utilizing singlet fission mechanisms, which is the material thickness. Moving forward, other effects the tetracene may have on the solar cell, such as moisture, UV light, etc., could be the focus of our future studies. On the other hand, future studies

also need to include other geographical factors, such as time of day, location of the solar panel, etc. into consideration.

Reference

(1) Adams, W. G.; Day, R. E. V. The action of light on selenium. *Proceedings of the Royal Society of London* **1997**, *25* (171-178), 113-117. DOI: 10.1098/rspl.1876.0024 (acccessed 2023/11/17).
(2) Chapin, D. M.; Fuller, C. S.; Pearson, G. L. A New Silicon p-n Junction Photocell for Converting Solar Radiation into Electrical Power. *Journal of Applied Physics* **2004**, *25* (5), 676-677. DOI: 10.1063/1.1721711 (acccessed 11/16/2023).
(3) States, U. U.S. Energy Information Administration (EIA). 2022.
(4) Shockley, W.; Queisser, H. J. Detailed Balance Limit of Efficiency of p-n Junction Solar Cells. *Journal of Applied Physics* **1961**, *32* (3), 510-519. DOI: 10.1063/1.1736034 (acccessed 2021/07/25).
(5) Roesch, R.; Faber, T.; von Hauff, E.; Brown, T. M.; Lira-Cantu, M.; Hoppe, H. Procedures and Practices for Evaluating Thin-Film Solar Cell Stability. *Advanced Energy Materials* **2015**, *5* (20), 1501407, https://doi.org/10.1002/aenm.201501407. DOI: https://doi.org/10.1002/aenm.201501407 (acccessed 2023/03/17).
(6) Fu, R.; Feldman, D.; Margolis, R. U.S. Solar Photovoltaic System Cost Benchmark Q1 2018. United States, 2019.
(7) Peña, M. A.; Fierro, J. L. G. Chemical Structures and Performance of Perovskite Oxides. *Chemical Reviews* **2001**, *101* (7), 1981-2018. DOI: 10.1021/cr980129f.
(8) Li, D.; Haneda, H.; Hishita, S.; Ohashi, N. Visible-Light-Driven N−F−Codoped TiO2 Photocatalysts. 2. Optical Characterization, Photocatalysis, and Potential Application to Air Purification. *Chemistry of Materials* **2005**, *17* (10), 2596-2602. DOI: 10.1021/cm049099p.
(9) Zhu, Y.; Liu, Y.; Miller, K. A.; Zhu, H.; Egap, E. Lead Halide Perovskite Nanocrystals as Photocatalysts for PET-RAFT Polymerization under Visible and Near-Infrared Irradiation. *ACS Macro Letters* **2020**, *9* (5), 725-730. DOI: 10.1021/acsmacrolett.0c00232.
(10) Xu, Y.-F.; Yang, M.-Z.; Chen, B.-X.; Wang, X.-D.; Chen, H.-Y.; Kuang, D.-B.; Su, C.-Y. A CsPbBr3 Perovskite Quantum Dot/Graphene Oxide Composite for Photocatalytic CO2 Reduction. *Journal of the American Chemical Society* **2017**, *139* (16), 5660-5663. DOI: 10.1021/jacs.7b00489.
(11) Wei, K.; Liang, B.; Sun, C.; Jiang, Y.; Yuan, M. Metal Halide Perovskites for Red-Emission Light-Emitting Diodes. *Small Structures* **2022**, *3* (10), 2200063, https://doi.org/10.1002/sstr.202200063. DOI: https://doi.org/10.1002/sstr.202200063 (acccessed 2023/02/14).
(12) Hu, Y.; Schlipf, J.; Wussler, M.; Petrus, M. L.; Jaegermann, W.; Bein, T.; Müller-Buschbaum, P.; Docampo, P. Hybrid Perovskite/Perovskite Heterojunction Solar Cells. *ACS Nano* **2016**, *10* (6), 5999-6007. DOI: 10.1021/acsnano.6b01535.
(13) Wu, Y.; Yang, X.; Chen, W.; Yue, Y.; Cai, M.; Xie, F.; Bi, E.; Islam, A.; Han, L. Perovskite solar cells with 18.21% efficiency and area over 1 cm2 fabricated by heterojunction engineering. *Nature Energy* **2016**, *1* (11), 16148. DOI: 10.1038/nenergy.2016.148.
(14) Turren-Cruz, S.-H.; Saliba, M.; Mayer, M. T.; Juárez-Santiesteban, H.; Mathew, X.; Nienhaus, L.; Tress, W.; Erodici, M. P.; Sher, M.-J.; Bawendi, M. G.; et al. Enhanced charge carrier mobility and lifetime suppress hysteresis and improve efficiency in planar perovskite solar cells. *Energy & Environmental Science* **2018**, *11* (1), 78-86, 10.1039/C7EE02901B. DOI: 10.1039/C7EE02901B.
(15) Liu, M.; Johnston, M. B.; Snaith, H. J. Efficient planar heterojunction perovskite solar cells by vapour deposition. *Nature* **2013**, *501* (7467), 395-398. DOI: 10.1038/nature12509.
(16) Nandasiri, M. I.; Shutthanandan, V.; Manandhar, S.; Schwarz, A. M.; Oxenford, L.; Kennedy, J. V.; Thevuthasan, S.; Henderson, M. A. Instability of Hydrogenated TiO2. *The Journal of Physical Chemistry Letters* **2015**, *6* (22), 4627-4632. DOI: 10.1021/acs.jpclett.5b02219.
(17) Schulze, P. S. C.; Bett, A. J.; Winkler, K.; Hinsch, A.; Lee, S.; Mastroianni, S.; Mundt, L. E.; Mundus, M.; Würfel, U.; Glunz, S. W.; et al. Novel Low-Temperature Process for Perovskite Solar Cells with a

Mesoporous TiO2 Scaffold. *ACS Applied Materials & Interfaces* **2017**, *9* (36), 30567-30574. DOI: 10.1021/acsami.7b05718.
(18) Chu, C.-W.; Li, S.-H.; Chen, C.-W.; Shrotriya, V.; Yang, Y. High-performance organic thin-film transistors with metal oxide/metal bilayer electrode. *Applied Physics Letters* **2005**, *87* (19), 193508. DOI: 10.1063/1.2126140 (acccessed 2021/07/25).
(19) Lian, J.; Lu, B.; Niu, F.; Zeng, P.; Zhan, X. Electron-Transport Materials in Perovskite Solar Cells. *Small Methods* **2018**, *2* (10), 1800082, https://doi.org/10.1002/smtd.201800082. DOI: https://doi.org/10.1002/smtd.201800082 (acccessed 2021/07/25).
(20) Sima, C.; Grigoriu, C.; Antohe, S. Comparison of the dye-sensitized solar cells performances based on transparent conductive ITO and FTO. *Thin Solid Films* **2010**, *519* (2), 595-597. DOI: https://doi.org/10.1016/j.tsf.2010.07.002.
(21) Yang, W. S.; Noh, J. H.; Jeon, N. J.; Kim, Y. C.; Ryu, S.; Seo, J.; Seok, S. I. High-performance photovoltaic perovskite layers fabricated through intramolecular exchange. *Science* **2015**, *348* (6240), 1234. DOI: 10.1126/science.aaa9272.
(22) Andreani, L. C.; Bozzola, A.; Kowalczewski, P.; Liscidini, M.; Redorici, L. Silicon solar cells: toward the efficiency limits. *Advances in Physics: X* **2019**, *4* (1), 1548305. DOI: 10.1080/23746149.2018.1548305.
(23) Al-Ashouri, A.; Köhnen, E.; Li, B.; Magomedov, A.; Hempel, H.; Caprioglio, P.; Márquez, J. A.; Morales Vilches, A. B.; Kasparavicius, E.; Smith, J. A.; et al. Monolithic perovskite/silicon tandem solar cell with >29% efficiency by enhanced hole extraction. *Science* **2020**, *370* (6522), 1300-1309. DOI: 10.1126/science.abd4016 (acccessed 2023/03/20).
(24) Čulík, P.; Brooks, K.; Momblona, C.; Adams, M.; Kinge, S.; Maréchal, F.; Dyson, P. J.; Nazeeruddin, M. K. Design and Cost Analysis of 100 MW Perovskite Solar Panel Manufacturing Process in Different Locations. *ACS Energy Letters* **2022**, *7* (9), 3039-3044. DOI: 10.1021/acsenergylett.2c01728.
(25) Wei, Z.; Chen, H.; Yan, K.; Yang, S. Inkjet Printing and Instant Chemical Transformation of a CH3NH3PbI3/Nanocarbon Electrode and Interface for Planar Perovskite Solar Cells. *Angewandte Chemie International Edition* **2014**, *53* (48), 13239-13243, https://doi.org/10.1002/anie.201408638. DOI: https://doi.org/10.1002/anie.201408638 (acccessed 2021/07/25).
(26) Kim, Y. Y.; Yang, T.-Y.; Suhonen, R.; Kemppainen, A.; Hwang, K.; Jeon, N. J.; Seo, J. Roll-to-roll gravure-printed flexible perovskite solar cells using eco-friendly antisolvent bathing with wide processing window. *Nature Communications* **2020**, *11* (1), 5146. DOI: 10.1038/s41467-020-18940-5.
(27) Yang, Y.; Hoang, M. T.; Bhardwaj, A.; Wilhelm, M.; Mathur, S.; Wang, H. Perovskite solar cells based self-charging power packs: Fundamentals, applications and challenges. *Nano Energy* **2022**, *94*, 106910. DOI: https://doi.org/10.1016/j.nanoen.2021.106910.
(28) Eperon, G. E.; Stranks, S. D.; Menelaou, C.; Johnston, M. B.; Herz, L. M.; Snaith, H. J. Formamidinium lead trihalide: a broadly tunable perovskite for efficient planar heterojunction solar cells. *Energy & Environmental Science* **2014**, *7* (3), 982-988, 10.1039/C3EE43822H. DOI: 10.1039/C3EE43822H.
(29) Noh, J. H.; Im, S. H.; Heo, J. H.; Mandal, T. N.; Seok, S. I. Chemical Management for Colorful, Efficient, and Stable Inorganic–Organic Hybrid Nanostructured Solar Cells. *Nano Letters* **2013**, *13* (4), 1764-1769. DOI: 10.1021/nl400349b.
(30) Da, Y.; Xuan, Y.; Li, Q. Quantifying energy losses in planar perovskite solar cells. *Solar Energy Materials and Solar Cells* **2018**, *174*, 206-213. DOI: https://doi.org/10.1016/j.solmat.2017.09.002.
(31) Huang, X.; Fu, H.; Chen, H.; Lu, Z.; Ding, D.; Zhao, Y. Analysis of loss mechanisms in InGaN solar cells using a semi-analytical model. *Journal of Applied Physics* **2016**, *119* (21), 213101. DOI: 10.1063/1.4953006 (acccessed 2021/07/25).
(32) König, D.; Casalenuovo, K.; Takeda, Y.; Conibeer, G.; Guillemoles, J. F.; Patterson, R.; Huang, L. M.; Green, M. A. Hot carrier solar cells: Principles, materials and design. *Physica E: Low-dimensional Systems and Nanostructures* **2010**, *42* (10), 2862-2866. DOI: https://doi.org/10.1016/j.physe.2009.12.032.

(33) Zhang, Y.; Jia, X.; Liu, S.; Zhang, B.; Lin, K.; Zhang, J.; Conibeer, G. A review on thermalization mechanisms and prospect absorber materials for the hot carrier solar cells. *Solar Energy Materials and Solar Cells* **2021**, *225*, 111073. DOI: https://doi.org/10.1016/j.solmat.2021.111073.
(34) Heidarzadeh, H.; Rostami, A.; Dolatyari, M. Management of losses (thermalization-transmission) in the Si-QDs inside 3C–SiC to design an ultra-high-efficiency solar cell. *Materials Science in Semiconductor Processing* **2020**, *109*, 104936. DOI: https://doi.org/10.1016/j.mssp.2020.104936.
(35) Blakers, A. W. Shading losses of solar-cell metal grids. *Journal of Applied Physics* **1992**, *71* (10), 5237-5241. DOI: 10.1063/1.350580 (acccessed 2021/07/25).
(36) Hannebauer, H.; Dullweber, T.; Baumann, U.; Falcon, T.; Brendel, R. 21.2%-efficient fineline-printed PERC solar cell with 5 busbar front grid. *physica status solidi (RRL) – Rapid Research Letters* **2014**, *8* (8), 675-679, https://doi.org/10.1002/pssr.201409190. DOI: https://doi.org/10.1002/pssr.201409190 (acccessed 2021/07/25).
(37) Du, Q. G.; Shen, G.; John, S. Light-trapping in perovskite solar cells. *AIP Advances* **2016**, *6* (6), 065002. DOI: 10.1063/1.4953336 (acccessed 2021/07/25).
(38) Foster, S.; John, S. Light trapping design for low band-gap polymer solar cells. *Optics Express* **2014**, *22* (S2), A465-A480. DOI: 10.1364/OE.22.00A465.
(39) Heidarzadeh, H. Effect of parasitic absorption of the plasmonic cubic nanoparticles on the performance of a plasmonic assisted halide thin-film perovskite solar cell. *Solar Energy* **2021**, *223*, 293-301. DOI: https://doi.org/10.1016/j.solener.2021.05.081.
(40) Xiao, Z.; Dong, Q.; Bi, C.; Shao, Y.; Yuan, Y.; Huang, J. Solvent Annealing of Perovskite-Induced Crystal Growth for Photovoltaic-Device Efficiency Enhancement. *Advanced Materials* **2014**, *26* (37), 6503-6509, https://doi.org/10.1002/adma.201401685. DOI: https://doi.org/10.1002/adma.201401685 (acccessed 2021/07/25).
(41) Zhang, M.; Yu, H.; Lyu, M.; Wang, Q.; Yun, J.-H.; Wang, L. Composition-dependent photoluminescence intensity and prolonged recombination lifetime of perovskite CH3NH3PbBr3−xClx films. *Chemical Communications* **2014**, *50* (79), 11727-11730, 10.1039/C4CC04973J. DOI: 10.1039/C4CC04973J.
(42) Ding, D.; Johnson, S. R.; Yu, S. Q.; Wu, S. N.; Zhang, Y. H. A semi-analytical model for semiconductor solar cells. *Journal of Applied Physics* **2011**, *110* (12), 123104. DOI: 10.1063/1.3671061 (acccessed 2021/07/25).
(43) Wang, Y.; Wu, T.; Barbaud, J.; Kong, W.; Cui, D.; Chen, H.; Yang, X.; Han, L. Stabilizing heterostructures of soft perovskite semiconductors. *Science* **2019**, *365* (6454), 687-691. DOI: 10.1126/science.aax8018 (acccessed 2023/03/31).
(44) McGovern, L.; Koschany, I.; Grimaldi, G.; Muscarella, L. A.; Ehrler, B. Grain Size Influences Activation Energy and Migration Pathways in MAPbBr3 Perovskite Solar Cells. *The Journal of Physical Chemistry Letters* **2021**, *12* (9), 2423-2428. DOI: 10.1021/acs.jpclett.1c00205.
(45) Wang, D.; Wright, M.; Elumalai, N. K.; Uddin, A. Stability of perovskite solar cells. *Solar Energy Materials and Solar Cells* **2016**, *147*, 255-275. DOI: https://doi.org/10.1016/j.solmat.2015.12.025.
(46) Leijtens, T.; Eperon, G. E.; Pathak, S.; Abate, A.; Lee, M. M.; Snaith, H. J. Overcoming ultraviolet light instability of sensitized TiO2 with meso-superstructured organometal tri-halide perovskite solar cells. *Nature Communications* **2013**, *4* (1), 2885. DOI: 10.1038/ncomms3885.
(47) Dualeh, A.; Gao, P.; Seok, S. I.; Nazeeruddin, M. K.; Grätzel, M. Thermal Behavior of Methylammonium Lead-Trihalide Perovskite Photovoltaic Light Harvesters. *Chemistry of Materials* **2014**, *26* (21), 6160-6164. DOI: 10.1021/cm502468k.
(48) Philippe, B.; Park, B.-W.; Lindblad, R.; Oscarsson, J.; Ahmadi, S.; Johansson, E. M. J.; Rensmo, H. Chemical and Electronic Structure Characterization of Lead Halide Perovskites and Stability Behavior under Different Exposures—A Photoelectron Spectroscopy Investigation. *Chemistry of Materials* **2015**, *27* (5), 1720-1731. DOI: 10.1021/acs.chemmater.5b00348.

(49) Niu, G.; Li, W.; Li, J.; Liang, X.; Wang, L. Enhancement of thermal stability for perovskite solar cells through cesium doping. *RSC Advances* **2017**, *7* (28), 17473-17479, 10.1039/C6RA28501E. DOI: 10.1039/C6RA28501E.
(50) Rolston, N.; Bush, K. A.; Printz, A. D.; Gold-Parker, A.; Ding, Y.; Toney, M. F.; McGehee, M. D.; Dauskardt, R. H. Engineering Stress in Perovskite Solar Cells to Improve Stability. *Advanced Energy Materials* **2018**, *8* (29), 1802139, https://doi.org/10.1002/aenm.201802139. DOI: https://doi.org/10.1002/aenm.201802139 (acccessed 2022/10/24).
(51) Choi, K.; Lee, J.; Choi, H.; Kim, G.-W.; Kim, H. I.; Park, T. Heat dissipation effects on the stability of planar perovskite solar cells. *Energy & Environmental Science* **2020**, *13* (12), 5059-5067, 10.1039/D0EE02859B. DOI: 10.1039/D0EE02859B.
(52) Jiang, Y.; Nielsen, M. P.; Baldacchino, A. J.; Green, M. A.; McCamey, D. R.; Tayebjee, M. J. Y.; Schmidt, T. W.; Ekins-Daukes, N. J. Singlet fission and tandem solar cells reduce thermal degradation and enhance lifespan. *Progress in Photovoltaics: Research and Applications* **2021**, *29* (8), 899-906, https://doi.org/10.1002/pip.3405. DOI: https://doi.org/10.1002/pip.3405 (acccessed 2022/11/21).
(53) Smith, M. B.; Michl, J. Singlet Fission. *Chemical Reviews* **2010**, *110* (11), 6891-6936. DOI: 10.1021/cr1002613.
(54) Pazos-Outón, L. M.; Lee, J. M.; Futscher, M. H.; Kirch, A.; Tabachnyk, M.; Friend, R. H.; Ehrler, B. A Silicon–Singlet Fission Tandem Solar Cell Exceeding 100% External Quantum Efficiency with High Spectral Stability. *ACS Energy Letters* **2017**, *2* (2), 476-480. DOI: 10.1021/acsenergylett.6b00678.
(55) United States. Department of Energy. Division of Chemical, S.; United States. Department of Energy. Office of Basic Energy, S. *Proceedings of the 27th DOE Solar Photochemistry Research Conference: Held at the Airlie Conference Center, Warrenton, Virginia, June 6-9, 2004*; United States Department of Energy Basic Energy Sciences Division, 2004.
(56) MacQueen, R. W.; Liebhaber, M.; Niederhausen, J.; Mews, M.; Gersmann, C.; Jäckle, S.; Jäger, K.; Tayebjee, M. J. Y.; Schmidt, T. W.; Rech, B.; et al. Crystalline silicon solar cells with tetracene interlayers: the path to silicon-singlet fission heterojunction devices. *Materials Horizons* **2018**, *5* (6), 1065-1075, 10.1039/C8MH00853A. DOI: 10.1039/C8MH00853A.
(57) Baldacchino, A. J.; Collins, M. I.; Nielsen, M. P.; Schmidt, T. W.; McCamey, D. R.; Tayebjee, M. J. Y. Singlet fission photovoltaics: Progress and promising pathways. *Chemical Physics Reviews* **2022**, *3* (2), 021304. DOI: 10.1063/5.0080250 (acccessed 2022/10/31).
(58) Chan, W.-L.; Ligges, M.; Zhu, X. Y. The energy barrier in singlet fission can be overcome through coherent coupling and entropic gain. *Nature Chemistry* **2012**, *4* (10), 840-845. DOI: 10.1038/nchem.1436.
(59) Paci, I.; Johnson, J. C.; Chen, X.; Rana, G.; Popović, D.; David, D. E.; Nozik, A. J.; Ratner, M. A.; Michl, J. Singlet Fission for Dye-Sensitized Solar Cells: Can a Suitable Sensitizer Be Found? *Journal of the American Chemical Society* **2006**, *128* (51), 16546-16553. DOI: 10.1021/ja063980h.
(60) Thomson, S. A. J.; Niklas, J.; Mardis, K. L.; Mallares, C.; Samuel, I. D. W.; Poluektov, O. G. Charge Separation and Triplet Exciton Formation Pathways in Small-Molecule Solar Cells as Studied by Time-Resolved EPR Spectroscopy. *The Journal of Physical Chemistry C* **2017**, *121* (41), 22707-22719. DOI: 10.1021/acs.jpcc.7b08217.
(61) D'Innocenzo, V.; Grancini, G.; Alcocer, M. J. P.; Kandada, A. R. S.; Stranks, S. D.; Lee, M. M.; Lanzani, G.; Snaith, H. J.; Petrozza, A. Excitons versus free charges in organo-lead tri-halide perovskites. *Nature Communications* **2014**, *5* (1), 3586. DOI: 10.1038/ncomms4586.
(62) Le, T. N.; Liu, L. Simulation for the Effect of Singlet Fission Mechanism of Tetracene on Perovskite Solar Cell. In *Energies*, 2023; Vol. 16.
(63) Asghar, M. I.; Zhang, J.; Wang, H.; Lund, P. D. Device stability of perovskite solar cells – A review. *Renewable and Sustainable Energy Reviews* **2017**, *77*, 131-146. DOI: https://doi.org/10.1016/j.rser.2017.04.003.

(64) Zhao, X.; Park, N.-G. Stability Issues on Perovskite Solar Cells. In *Photonics*, 2015; Vol. 2, pp 1139-1151.
(65) Xia, J.; Sanders, S. N.; Cheng, W.; Low, J. Z.; Liu, J.; Campos, L. M.; Sun, T. Singlet Fission: Progress and Prospects in Solar Cells. *Advanced Materials* **2017**, *29* (20), 1601652, https://doi.org/10.1002/adma.201601652. DOI: https://doi.org/10.1002/adma.201601652 (acccessed 2022/10/24).
(66) Wu, T. C.; Thompson, N. J.; Congreve, D. N.; Hontz, E.; Yost, S. R.; Van Voorhis, T.; Baldo, M. A. Singlet fission efficiency in tetracene-based organic solar cells. *Applied Physics Letters* **2014**, *104* (19), 193901. DOI: 10.1063/1.4876600 (acccessed 2022/10/24).
(67) Paulescu, M.; Schlett, Z. A simplified but accurate spectral solar irradiance model. *Theoretical and Applied Climatology* **2003**, *75* (3), 203-212. DOI: 10.1007/s00704-003-0731-y.
(68) Francisco-López, A.; Charles, B.; Weber, O. J.; Alonso, M. I.; Garriga, M.; Campoy-Quiles, M.; Weller, M. T.; Goñi, A. R. Equal Footing of Thermal Expansion and Electron–Phonon Interaction in the Temperature Dependence of Lead Halide Perovskite Band Gaps. *The Journal of Physical Chemistry Letters* **2019**, *10* (11), 2971-2977. DOI: 10.1021/acs.jpclett.9b00876.
(69) Qin, P.; Tanaka, S.; Ito, S.; Tetreault, N.; Manabe, K.; Nishino, H.; Nazeeruddin, M. K.; Grätzel, M. Inorganic hole conductor-based lead halide perovskite solar cells with 12.4% conversion efficiency. *Nature Communications* **2014**, *5* (1), 3834. DOI: 10.1038/ncomms4834.
(70) Nakka, L.; Cheng, Y.; Aberle, A. G.; Lin, F. Analytical Review of Spiro-OMeTAD Hole Transport Materials: Paths Toward Stable and Efficient Perovskite Solar Cells. *Advanced Energy and Sustainability Research* **2022**, *3* (8), 2200045, https://doi.org/10.1002/aesr.202200045. DOI: https://doi.org/10.1002/aesr.202200045 (acccessed 2023/02/14).
(71) 98/01426 Statistical analysis of the Angström formula coefficients and application for Turkey: Sahin, A. D. and Sen, Z. Solar Energy, 1998, 62, (1), 29–38. *Fuel and Energy Abstracts* **1998**, *39* (2), 125. DOI: https://doi.org/10.1016/S0140-6701(98)97568-3.
(72) Kulkarni, S. A.; Baikie, T.; Boix, P. P.; Yantara, N.; Mathews, N.; Mhaisalkar, S. Band-gap tuning of lead halide perovskites using a sequential deposition process. *Journal of Materials Chemistry A* **2014**, *2* (24), 9221-9225, 10.1039/C4TA00435C. DOI: 10.1039/C4TA00435C.
(73) Starr, D. E.; Sadoughi, G.; Handick, E.; Wilks, R. G.; Alsmeier, J. H.; Köhler, L.; Gorgoi, M.; Snaith, H. J.; Bär, M. Direct observation of an inhomogeneous chlorine distribution in CH3NH3PbI3−xClx layers: surface depletion and interface enrichment. *Energy & Environmental Science* **2015**, *8* (5), 1609-1615, 10.1039/C5EE00403A. DOI: 10.1039/C5EE00403A.
(74) Tetracene. ChemSpider: 2022.
(75) Haeger, T.; Heiderhoff, R.; Riedl, T. Thermal properties of metal-halide perovskites. *Journal of Materials Chemistry C* **2020**, *8* (41), 14289-14311, 10.1039/D0TC03754K. DOI: 10.1039/D0TC03754K.
(76) Tabor, D. Mechanical *P*roperties *o*f

*E*nergetic *M*aterials. Physics *&* *C*hemistry *o*f *S*olids *C*avandish *L*abatory, 1977.
(77) Lopez-Varo, P.; Amara, M.; Cacovich, S.; Julien, A.; Yaïche, A.; Jouhari, M.; Rousset, J.; Schulz, P.; Guillemoles, J.-F.; Puel, J.-B. Dynamic temperature effects in perovskite solar cells and energy yield. *Sustainable Energy & Fuels* **2021**, *5* (21), 5523-5534, 10.1039/D1SE01381E. DOI: 10.1039/D1SE01381E.
(78) Thermal Coefficients.
(79) Pisoni, A.; Jaćimović, J.; Barišić, O. S.; Spina, M.; Gaál, R.; Forró, L.; Horváth, E. Ultra-Low Thermal Conductivity in Organic–Inorganic Hybrid Perovskite CH3NH3PbI3. *The Journal of Physical Chemistry Letters* **2014**, *5* (14), 2488-2492. DOI: 10.1021/jz5012109.
(80) Zhang, H.; Brill, J. W. Interlayer thermal conductivity of rubrene measured by ac-calorimetry. *Journal of Applied Physics* **2013**, *114* (4), 043508. DOI: 10.1063/1.4816468 (acccessed 2023/04/12).

(81) Tanaka, K.; Takahashi, T.; Ban, T.; Kondo, T.; Uchida, K.; Miura, N. Comparative study on the excitons in lead-halide-based perovskite-type crystals CH3NH3PbBr3 CH3NH3PbI3. *Solid State Communications* **2003**, *127* (9), 619-623. DOI: https://doi.org/10.1016/S0038-1098(03)00566-0.
(82) Hirst, L. C.; Ekins-Daukes, N. J. Fundamental losses in solar cells. *Progress in Photovoltaics: Research and Applications* **2011**, *19* (3), 286-293, https://doi.org/10.1002/pip.1024. DOI: https://doi.org/10.1002/pip.1024 (acccessed 2023/01/13).